Nat. Hazards Earth Syst. Sci. Discuss., https://doi.org/10.5194/nhess-2018-319
Manuscript under review for journal Nat. Hazards Earth Syst. Sci.
Discussion started: 23 November 2018


Natural Hazards and Earth System Sciences
Open Access
Discussions

# The impact of lightning and radar data assimilation on the performance of very short term rainfall forecast for two case studies in Italy

Stefano Federico[1], Rosa Claudia Torcasio[2], Elenio Avolio[2], Olivier Caumont[3], Mario Montopoli[1], Luca Baldini[1], Gianfranco Vulpiani[4], Stefano Dietrich[1]

1. ISAC-CNR, via del Fosso del Cavaliere 100, Rome, Italy
2. ISAC-CNR, zona Industriale comparto 15, 88046 Lamezia Terme, Italy
3. CNRM UMR 3589, University of Toulouse, Météo-France, CNRS, 42 avenue G. Coriolis, 31057 Toulouse, France
4. Dipartimento Protezione Civile Nazionale Ufficio III - Attività Tecnico Scientifiche per la Previsione e Prevenzione dei Rischi, 00189 Rome

**Abstract**

In this paper, we study the impact of the lightning and radar reflectivity factor data assimilation on the precipitation VSF (Very Short-term Forecast, 3 hours in this study) for two relevant case studies occurred in Italy. The first case refers to a moderate localised rainfall over Central Italy happened on 16 September 2017. The second case, occurred on 9 and 10 September 2017, was very intense causing damages in several geographical areas, especially in Livorno (Tuscany) where 9 people lost their life.

The first case study was missed by several operational forecasts (from both public and private sectors), including that performed by the model used in this paper, while the Livorno case was partially predicted by operational models.

We use the RAMS@ISAC model (Regional Atmospheric Modelling System at Institute for Atmospheric Sciences and Climate of the Italian National Research Council), whose 3D-Var extension to the assimilation of RADAR reflectivity factor is shown in this paper.

Results for the two cases show that the assimilation of lightning and radar reflectivity factor, especially when used together, have a significant and positive impact on the precipitation forecast. The improvement compared to the control model, not assimilating lightning and radar reflectivity factor, is systematic because occurs for all the Very Short-term Forecast (VSF, 3h) of the events considered.

For specific time intervals, the data assimilation is of practical importance for civil protection purposes because it transforms a missed forecast of intense precipitation (> 40 mm/3h) in a correct forecast.

While there is an improvement of the rainfall VSF thanks to the lightning and radar reflectivity factor data assimilation, its usefulness is partially reduced by the increase of the false alarms in the forecast assimilating both types of data.

## 1. Introduction

Initial conditions of numerical weather prediction (NWP) models are a key point for a good forecast (Stensrud and Fritsch, 1994; Alexander et al., 1999). Nowadays limited area models are operational at the resolution of few kilometres (< 5 km) and data assimilation of asynoptic local observations is crucial to correctly represent the state of the atmosphere at local scale (Weisman et al., 1997; Weygandt et al., 2008). This is especially important over the sea, where the absence of local observations and model deficiencies can misrepresent convection.

The assimilation of the radar reflectivity factor is important to improve the weather forecast because, being the reflectivity factor related to both the hydrometeors types and size, it can add information and eventually change the weather forecast. This is particularly important considering the high repetition rate (asynoptic data) and the high spatial resolution (local scale) of the radar data.

The first attempts to assimilate the radar reflectivity factor are reported in Sun and Crook (1997, 1998), who expanded VDRAS (Variational Doppler Radar Analysis System) to include microphysical retrieval. Following these studies several systems to assimilate radar observations, both Doppler velocity and reflectivity factor, were developed (Xue et al., 2003, Zhao et al., 2006; Xu et al., 2010). All these studies showed the stability and robustness of assimilating radar observations as well as an improvement to the weather forecast.

Radar data are also assimilated in WRF (Weather Research and Forecasting, Skamarock et al., 2008; Barker et al., 2012) model both using 3DVar (Xiao et al., 2005, 2007; Barker et al., 2004) and 4DVar approaches (Wang et al., 2013; Sun and Wang, 2012). The capability to assimilate radar data into WRF was recently applied to a heavy rainfall event over Central Italy by Maiello et al. (2014). They showed a notable and positive impact of the radar data assimilation on the precipitation forecast, also when radar data are assimilated together with conventional data.

In addition to those methods, which assimilate the radar reflectivity factor directly perturbing the hydrometeor contents predicted by the forecast models, there are indirect methods that aim at modifying other variables. In particular, the method proposed by Caumont et al. (2010) acts on the relative humidity filed. It consists of two different steps: a 1D retrieval of relative humidity (pseudo-profile), which depends on the radar reflectivity factor observations, followed by 3D-Var assimilation of the pseudo-profile. This method, though less direct than perturbing hydrometeors, has the advantage to reduce the computational cost at the kilometric scale, and to avoid questionable assumptions of the direct methods.

The choice of updating the moisture field directly is motivated by its greater impact on analyses and forecasts in comparison to that of hydrometeor-related quantities (e.g., Fabry and Sun, 2010). Caumont et al. (2010) showed that the method was able to improve the weather prediction for a case of heavy precipitation in southern France and for eight-day long assimilation cycle.

The method was applied in other studies (Wattrelot et al., 2014; Ridal and Dalbom, 2016; Muller et al., 2017), or modified using 4D-Var in place of 3D-Var (Ikuta and Honda, 2011) showing in all cases its capability to improve the weather forecast. The method is also used in the operational context (Wattrelot et al., 2014).

Lightning are another important source of asynoptic data due to their ability to locate precisely the convection with few temporal gaps as well as, availability in real time thanks to the low bandwidth required for data transfer (Mansell et al., 2007). For these reasons, in the last two decades, there have been attempts to assimilate lightning into meteorological models both at low horizontal resolution, which need a cumulus parameterization scheme to simulate convection, and at convection permitting scales.

The first attempts to assimilate lightning in numerical weather prediction models (NWP) were based on relationships between lightning and rainfall rate estimated by microwave sensors on board polar satellites (Alexander et al., 1999; Chang et al., 2001; Jones and Macpherson, 1997). In this approach, the rainfall rate was computed as a function of lightning observations and then transformed into latent heat, which was assimilated. The results of these studies showed a positive impact of the lightning data assimilation on the forecast up to 24h also for fields at the large scale, as sea-level pressure, encouraging further researches.

Mansell et al. (2007) modified the Kain-Fritsch (Kain and Fritsch, 1993) cumulus convective scheme to force convection when/where flashes are observed while the convective scheme was not activated in the model simulation, demonstrating the potential of lightning to correctly locate the convection. A similar approach was introduced by Giannaros et al. (2016) into the WRF model showing the positive impact of the lightning data assimilation on the precipitation forecast up to 24h for eight convective events occurred over Greece.

Fierro et al. (2012) introduced a methodology to assimilate lightning by modifying the water vapour mixing ratio simulated by the model according to a function depending on the flash-rate and on the simulated graupel mixing ratio. The water vapour could be assimilated by nudging (Fierro et al., 2012) or 3D-Var (Fierro e al., 2016).

Qie et al. (2014) extended the methodology of Fierro et al. (2012) to assimilate ice crystals, graupel and snow, showing promising results for deep convective events in China.

Federico et al. (2017a) implemented the methodology of Fierro et al. (2012) in RAMS@ISAC model, obtaining the systematic and significant improvement of the precipitation forecast at the very short range (3h) for twenty case studies occurred over Italy; the impact of lightning data assimilation for longer time ranges (6h-24h; Federico et al., 2017b) showed a considerable impact on the 6h precipitation forecast, with smaller (negligible) effects at 12 h (24 h).

In this paper we study the impact of the radar reflectivity factor and lightning observations data assimilation on the very short term (3h) rainfall prediction of two case studies over Italy. We use the method of Federico et al. (2017a) to assimilate lightning and the method of Caumont et al. (2010) to assimilate the radar reflectivity factor. The case studies occurred on September 2017. The first case, named Serano case, occurred on 16 September, was characterized by moderate-intense and localized rainfall. The second case, named Livorno case, occurred on 09-10 September was characterized by deep convection and very intense precipitation in several parts of Italy. Even if the Livorno case occurred before the Serano case, we will reverse the chronological occurrence in the discussion, ordering the event from the less intense to the most intense.

The Serano case was missed by the control forecast, not assimilating radar reflectivity factor and lightning. The Livorno event was partially predicted by the control forecast, which missed the abundant precipitation over Central Italy (see Section 4), and predicted the intense precipitation over Livorno delayed compared to the observations.

With respect to previous works, this study investigates the benefits brought by the combined use of radar and lightning observations into RAMS@ISAC, paving the way to systematic improvements of weather forecasts.

This paper is organized as follows: Section 2 gives details on the synoptic environment of the case studies showing daily precipitation, lightning and, for specific times, radar observations; Section 3 gives details on the meteorological model, lightning and radar data assimilation; Section 4 shows the results for five very short-term forecast (VSF), two for Serano and three for Livorno; Discussion and conclusions are given in Section 5.

## 2. The case studies

### *2.1 The 16 September 2017 (Serano) case study*

Nat. Hazards Earth Syst. Sci. Discuss., https://doi.org/10.5194/nhess-2018-319
Manuscript under review for journal Nat. Hazards Earth Syst. Sci.
Discussion started: 23 November 2018


During the 16 September 2017 the whole Italian country was under the influence of a cyclone that developed on the lee of the Alps. The storm crossed Italy from NW to SE leaving light precipitation over most of the peninsula with moderate rainfall over Central Italy. Figure 1 shows the precipitation recorded by the Italian raingauge network on 16 September 2017. A light precipitation (below 5 mm/day) is reported by 1018 raingauges out of the 1666 stations measuring precipitation ($\geq$ 0.2 mm/day) on this day. Fourteen stations over Central Italy recorded more than 50 mm/day and 6 stations more than 60 mm/day. The maximum precipitation on this day was 90 mm/day in Città di Castello (Umbria Region). Because the meteorological radar closest to the maximum precipitation is over Serano mountain, hereafter this event will be referred as Serano.

The synoptic condition during the event is shown in Figure 2. At 500 hPa (Figure 2a) a trough, elongated in the SW-NE direction, extends over Western Europe and air masses are advected from the SW towards the western Alps. The interaction between the airflow and the Alps generates a low pressure, at low levels, on the lee of the Alps over Northern Italy.

The situation at the surface (Figure 2b) shows the meteorological front represented by the equivalent potential temperature gradient between air masses advected over the Mediterranean Sea from NW and air masses advected from the South over the Tyrrhenian Sea, as a consequence of the pressure pattern that forms over the area. It is also notable the feeding of warm unstable air masses towards Central Italy.

Infrared satellite images (Figure 3), from 00 UTC on 16 September to 00 UTC on 17 September 2017, show the cold front structure moving slowly from NW towards SE. Interestingly, at 00 UTC on 16 September, it is apparent a well-defined cloud system over Central Italy (red circle of Figure 3a), which produced most of the daily precipitation observed between 43.50 and 45.0 N in the six-hours between 00 UTC and 06 UTC on 16 September 2017.

The well-defined cloud system over Central Italy is also clear in the radar Constant Altitude Plan Position Indicator (CAPPI) at 3 km above sea level at 02 UTC on 16 September (Figure 4). This CAPPI is formed by interpolating all the available data from the federated Italian radar network coordinated by the Department of Civil Protection (twenty-two radars, see Section 3.3 for their positions) and it is also referred as the national radar composite (hereafter also mosaic). Several convective cells exceeding 35 dBz can be noted on on central-northern Italy. Importantly, the cloud system over Central Italy shown by the satellite infrared channel at 00 UTC (Figure 3a) and that of the CAPPI at 02 UTC have a similar position, and the cloud system insisted for several hours over Central Italy (00-06 UTC).

Figure 5 shows the lightning recorded by the LINET network (Betz et al., 2009) on 16 September 2017. More than 60.000 flashes were recorded for the whole day; most of them occurred during the afternoon and evening (the peak of more than 8000 flashes in one hour was at 22 UTC), but a secondary maximum occurred during the night on 16 September, form 00 UTC to 06 UTC. In this phase more than 2000 flashes were observed in Central Italy (see the green-blue dots in Figure 5). From lightning observations, it follows that the storm had two main phases over Central Italy: the first one occurred during the night (00-06 UTC) and was characterised by the most intense rainfall; the second started after 18 UTC. In Section 4 one VSF for each phase will be considered.

### *2.2 The 09-10 September 2017 (Livorno) case study*

During the days 09 and 10 September 2017, Italy was hit by a severe storm characterised by intense and widespread rainfall over the country. Damages to property were reported in several parts of Italy, while nine people died around Livorno, in Tuscany for causes related to the storm.

Figure 6a shows the precipitation on 09 September recorded by the Italian raingauge network. Rainfall was more intense over the Alps, where the maximum daily precipitation was observed (193 mm/day) and over Liguria, with precipitation of the order of 30-50 mm/day. One station over Tuscany reported 90 mm/day, showing that intense precipitation already started over the Region. The intensity of the storm on 09 September was high because 20 raingauges reported more than 100 mm/day and 70 raingauges more than 60 mm/day, and, in most cases, this precipitation occurred in few hours. For example, the precipitation over Tuscany fell in the last 6 h of the day.

The following day (see Figure 6b) had higher rainfall. Precipitation occurred mainly over Central Italy, especially over Lazio, and over Northern Italy, in particular the North-East. In Tuscany, the two stations close to the sea, in the Livorno area, recorded about 150 mm/day mostly fallen in the hours between 00 and 06 UTC. The rainfall on 10 September was abundant: 256 stations out of 2065 stations reported more than 60 mm/day, 60 of which recorded more than 100 mm/day.

Synoptic conditions leading to this storm are represented by the situation at 00 UTC on 10 September, shown in Figure 7, when the storm was already producing precipitation over Northern Italy. At 500 hPa (Figure 7a) a trough extends from Northern Europe towards the Mediterranean. The interaction between air-masses and Western Alps generates a depression on the lee of the

Nat. Hazards Earth Syst. Sci. Discuss., https://doi.org/10.5194/nhess-2018-319
Manuscript under review for journal Nat. Hazards Earth Syst. Sci.
Discussion started: 23 November 2018


Alps, over Northern Italy, which, in the following hours, crossed the whole peninsula from NW to SE. It is also noted the divergent flow over Central and Northern Italy favouring upward motions.
At the surface, Figure 7b, it is apparent the equivalent temperature gradient over the western Mediterranean caused by the contrast between air masses pre-existing over the sea and air masses advected from France towards the Mediterranean Sea. The cyclonic circulation over the Ligurian Sea is forced by the low-pressure over the Northern Italy. The pressure field at the surface advects air masses from the South over the Tyrrhenian Sea. These air masses are unstable, i.e. humid and warm, and feed the cyclone during its development.
From the synoptic point of view, this storm and the Serano case are similar and represent two cyclones developing on the lee of the Alps (Buzzi and Tibaldi, 1978). However, the Livorno case is more intense than Serano as shown by the larger rainfall, as well as by the more unstable air masses over the Tyrrhenian Sea that characterise the Livorno case.
The notable intensity of the Livorno case is also confirmed by the lightning distribution (Figure 8). During the evening on 9 September (after 18 UTC) about 38.000 flashes were associated with the propagation of the storm from NW to SE. On 10 September about 170.000 flashes were recorded along Italy, following the movement of the storm propagating from NW to SE. So, more than 200.000 flashes were recorded from 18 UTC on 09 September to 00 UTC on 11 September, which are more than twice those recorded for Serano.
Satellite images (thermal infrared channel, 10.8 micron; Figure 9) show the extension of the cloud coverage every 12 hours. It is well evident the cloud system associated with the cold front that extends over Europe and moves from north-west to south-east. More specifically, the satellite image at 00 UTC shows the cloud system over Livorno area (red circle in Figure 9b), before the main precipitation event over Tuscany (00-06 UTC), while Figure 9c shows the cloud system over Central Italy (orange circle), at the end of the period of intense precipitation over Lazio (06-12 UTC).
We conclude the synoptic analysis of the case study with two CAPPI at 3 km observed by the radar network of the Department of Civil Protection. The CAPPI of Figure 10a, at 00 UTC on 10 September, shows the cloud system over Tuscany with reflectivity factor up to 40 dBz. Other clouds are producing rainfall over northern Italy. The cloud system remained stationary over Tuscany for the period 00-06 UTC, with new cells developing over the sea and moving towards the land for six hours, causing the flood in Livorno. The CAPPI of Figure 10a is the last assimilated by the VSF of 00-03 UTC on 10 September shown in Section 4.

Figure 10b shows the CAPPI of the national radar mosaic at 3 km above the sea level and at 06 UTC. The cloud system is moving towards Central Italy with reflectivity up to 45 dBz. Other cloud systems are apparent over northern Italy. Figures 10a-10b well represents the movement of the storm towards SE and Figure 10b shows the last CAPPI assimilated by the 06-09 UTC VSF shown in Section 4.

## 3.Data and Methods

### *3.1 RAMS@ISAC and simulations set-up*

The RAMS@ISAC is used for the numerical experiments of this work. The model is based on the RAMS 6.0 model (Cotton et al., 2003) with the addition of four main features, as well as a number of minor improvements. First, it implements additional single moment microphysical schemes, whose performance is shown in Federico (2016): among them, the WSM6 (Hong and Lim, 2006) is used in this paper. Second, it predicts the occurrence of lightning following the methodology of Dahl et al. (2012), and the implementation and performance of the scheme is discussed in Federico et al. (2014). Third, the model can assimilate lightning through nudging (Fierro et al., 2012; Federico et al., 2017a). Forth, the model implements a 3D-Var data assimilation system (Federico, 2013, hereafter also RAMS-3DVar), whose extension to the radar reflectivity factor is shown in this paper (Section 3.3).

The list of the main physical parameterisation schemes used in the simulations of the RAMS@ISAC discussed in this paper is shown in Table 1.

Considering the domains and the configuration of the grids (Figure 11 and Table 2), two different set-ups are used for Serano and Livorno. For the first case, we use the domains D1 and D2, while for Livorno we use also the third domain D3. The first domain covers a large part of Europe and extends over the North Africa. For this domain, the horizontal resolution of the grid is 10 km (R10). The second domain extends over the whole Italy and part of Europe and the grid has 4 km horizontal resolution (R4). The third domain covers the Tuscany Region, has 4/3 km horizontal resolution (R1), and it is used for Livorno to represent with more detail the precipitation field.

The resolutions and the extensions of the grids in the vertical direction are the same for the three domains and cover the troposphere and the lower stratosphere.

The nesting between the first and second domains is one-way, while the nesting between the second and the third domains is two-ways.

The VSF is implemented as shown in Figure 12. First a run using the R10 configuration is performed using the GFS analysis/forecast cycle issued at 12 UTC as initial and boundary conditions. This run, which starts at 12 UTC on 16 September for Serano and at 12 UTC on 09 September for Livorno, lasts 36 h and doesn't assimilate radar reflectivity factor or lightning.
Starting from 12 UTC, ten VSF are performed using R4 (for Serano) or both R4 and R1 (for Livorno). The VSF lasts 9h and uses R10 simulation as initial and boundary conditions (one-way nesting). The 9h forecast is divided into two parts: the first six hours are the assimilation stage when the assimilated source of observations are continuously used to constrain the VSF to the observations whereas the last three hours are dedicated to the forecast stage when the VSF freely evolve without external constrains. During the assimilation stage, flashes are assimilated with the nudging technique (Section 3.2), while radar reflectivity is assimilated every one-hour by the Caumont et al. (2010) method (Section 3.3).
It is noted that data assimilation is performed in the domain D2 (R4) only, and the innovations are transferred to the domain D3 (R1), for the Livorno case, by the two way-nesting.
The verification of the VSF for precipitation is done by visual comparison of the model output with the raingauge network of the Department of Civil Protection, which has more than 3000 raingauges all over Italy (Davolio et al., 2015).
In addition we consider the FBIAS (Frequency Bias; range [0, + ∞) ), where 1 is the perfect score, i.e. when no misses and false alarms occur), POD (Probability of Detection; range [0, 1], where 1 is the perfect score and 0 the worst value), ETS (Equitable Threat Score; range [-1/3,1], where 1 is the perfect score and 0 is a useless forecast) and HR (Hit Rate or correct proportion; range [0, 1], where 1 is the perfect score and 0 the worst value) computed from 2x2 dichotomous contingency tables (Wilks, 2006) for different rainfall thresholds (0.2 mm/3h, 1mm/3h and from 2mm/3h to the maximum thresholds, i.e. 40 mm/3h for Serano and 60 mm/3h for Livorno, every 2 mm/3h). In particular, defining the hits (*a*, a hit occurs when both the precipitation forecast and the corresponding raingauge observation are above or equal to a rainfall threshold), false alarms (*b*, a false alarm occurs when the precipitation forecast is above or equal to a rainfall threshold, while the corresponding raingauge observation is below the threshold); misses (*c*, a missing occurs when the forecast precipitation is below a rainfall threshold, while the corresponding raingauge observation is above or equal to the threshold); (*d*, a correct no forecast occurs when both the precipitation forecast and the corresponding observation are below a rainfall threshold), we have:

$$FBIAS = \frac{a+b}{a+c}$$
$$POD = \frac{a}{a+c}$$
$$ETS = \frac{a-a_r}{a+b+c-a_r}; \quad a_r = \frac{(a+b)(a+c)}{a+b+c+d} \qquad (1)$$
$$HR = \frac{a+d}{a+b+c+d}$$

where $a_r$ is the probability to have a correct forecast by chance (Wilks, 2006) .The hits, false alarms, misses and correct no forecast are computed comparing the precipitation forecast at four RAMS@ISAC grid points surrounding a raingauge and taking among them the closest value to the raingauge measurement (nearest-neighbour). In this way, we tolerate a spatial error of $D*(2)^{1/2}$ for the rainfall forecast, where $D$ is the model grid spacing (4 km or 4/3 km depending by the case considered). Because the scores are computed for the second and third RAMS@ISAC domains, we tolerate spatial errors of 5.7 km and 1.9 km, respectively.

### *3.2 Lightning data assimilation*

The lightning data assimilation scheme, introduced in previous papers (Federico et al., 2017a; 2017b), is shown here for completeness.

The method starts by computing the water vapour mixing ratio $q_v$:

$$q_v = Aq_s + Bq_s \tanh(CX)(1-\tanh(Dq_s^{\alpha})) \qquad (2)$$

Where coefficients are set to A=0.86, B=0.15, C=0.30 D=0.25, $\alpha$=2.2, $q_s$ is the saturation mixing ratio at the model atmospheric temperature, and $q_g$ is the graupel mixing ratio (g $kg^{-1}$). $X$ is the number of flashes falling in a grid box of domain D2 (R4) in the past five minutes. The mixing ratio $q_v$ of Eq. (2) is computed only for grid points where flashes are recorded, i.e. $X$ is greater than zero. More specifically, for each grid point we consider the number of flashes falling in a grid box centred at the grid point in the last five minutes. The mixing ratio of Eqn. (2) is compared with that predicted by the model. If the mixing ratio of Eqn. (2) is larger than the simulated one, the latter is changed with the value given by Eqn. (2), otherwise the modelled mixing ratio is left unchanged. This method can only add water vapour to the forecast.

The check and eventual substitution of the water vapor is performed every five minutes and it is made only in the charging zone (0 °C, -25°C).

Lightning data are provided by the LINET network, which has more than 500 sensors over worldwide with the greatest density over Europe.

### *3.3 Radar data assimilation*

The method assimilates radar CAPPI that are operationally provided by the Italian Department of Civil Protection (DPC). Radar data are provided over a regular Cartesian grid with 1 km horizontal resolution and for three vertical levels (2, 3, 5 km above the sea level) and radar observations can be considered as vertical profiles. These CAPPIs at the three different altitudes of 2, 3, and 5km can be considered as under-sampled vertical profiles. CAPPIs are composed starting from the 22 radars of the Italian Radar Network (Figure 13) 19 operating at the C-band (i.e., 5.6 GHz) and 3 at X-band (i.e., 9.37 GHz). Data quality control and CAPPI composition is performed by DPC and no additional quality control is applied in this paper. Before entering the data assimilation, the Cartesian grid is reduced to 5 by 5 km by choosing one point every five of the Cartesian grid provided by DPC in order to reduce the dimensionality of the problem and to account, at least in part, for the correlation error of the observations.

The methodology to assimilate radar reflectivity factor is that of Caumont et al. (2010), named 1D+3DVar, which is a two-step process: first, using a Bayesian approach inspired to GPROF (Olson et al., 1996; Kummerow et al., 2001), 1D pseudo-profiles of model variables are computed, then those pseudo-profiles are assimilated by 3DVar. Both steps are discussed shortly.

The first step computes a pseudo-profile of relative humidity weighting the model profiles of relative humidity around the radar profile (Bayesian approach). In particular:

$$\mathbf{z}_{\mathbf{o}}^{\mathbf{p}} = \frac{\sum_i \mathbf{RH}_{\mathbf{i}} W_i}{\sum_j W_j} \quad (3)$$

Where $RH_i$ is the RAMS@ISAC vertical profile of relative humidity at a grid point inside a square of 50*50 km$^2$ centred at the radar vertical profile, $W_i$ is the weight of each profile and $\mathbf{z_o}^{\mathbf{p}}$ is the relative humidity pseudo-profile. The summation is taken over all the grid points inside a square of 50*50 km$^2$ around the observed profile and the denominator is a normalisation factor. The weights are determined considering the agreement between the simulated and observed reflectivity factor:

$$W_i = \exp\left\{-\frac{1}{2}\left[\mathbf{z}_{\mathbf{o}} - h_z(x_i)\right]^T \mathbf{R}_{\mathbf{z}}^{-1}\left[\mathbf{z}_{\mathbf{o}} - h_z(x_i)\right]\right\} \quad (4)$$

Where $h_z$ is the forward observation operator, transforming the background column $\mathbf{x_i}$ into the observed reflectivity factor. The forward observation operator is specific for the WSM6

Nat. Hazards Earth Syst. Sci. Discuss., https://doi.org/10.5194/nhess-2018-319
Manuscript under review for journal Nat. Hazards Earth Syst. Sci.
Discussion started: 23 November 2018

Natural Hazards and Earth System Sciences
Discussions
Open Access

microphysics scheme and is available in WRF release 3.8. It assumes Marshall-Palmer hydrometeors size-distribution, Rayleigh scattering, and depends on the mixing ratios of rain, graupel and snow.

The observation error matrix $\mathbf{R_z}$ in Eqn. (4) is assumed diagonal, i.e. observation errors are uncorrelated, and its value is $n\sigma^2$, where $\sigma$ is 1 dBz and $n$ is the number of available observations in the vertical profile (from 1 to 3).

It is important to note that the method is not able to force convection when the model has no rain, snow and graupel in a square around (50*50 km$^2$) a specific radar profile with reflectivity factor greater than zero. In this case, the pseudo profile of relative humidity is assumed saturated above the condensation level and with no data below to force convection into the model.

It is also noted that the method is able to dry the model when the reflectivity factor is simulated but not observed, by giving more weight to the drier relative humidity profiles simulated by RAMS@ISAC in Eqn. (3).

The pseudo-profiles computed with the procedure introduced above, are then used as observations in the RAMS-3DVar data assimilation (Federico, 2013), minimising the cost-function:

$$J(\mathbf{x}) = \frac{1}{2}(\mathbf{x}-\mathbf{x_b})^T \mathbf{B}^{-1}(\mathbf{x}-\mathbf{x_b}) + \frac{1}{2}(\mathbf{y_o}-h(\mathbf{x}))^T \mathbf{B}^{-1}(\mathbf{y_o}-h(\mathbf{x})) \quad (5)$$

Where $\mathbf{x}$ is the state vector giving the analysis when $J$ is minimized, $\mathbf{x_b}$ is the background, $\mathbf{B}$ and $\mathbf{R}$ are the background and observations error matrices, $\mathbf{y_o}$ is the observation vector and $h$ is the forward observation operator transforming the state vector into observations. The cost function in RAMS-3DVar is implemented in incremental form (Courtier et al., 1994; see Federico 2013 for the details).

The background error matrix is computed using the NMC method (Parrish and Derber, 1992; Barker et al. 2004) applied to the HyMeX-SOP1 (Hydrological cycle in the Mediterranean Experiment – First Special Observing Period occurred in the period 6 September-6 November 2012; Ducroq et al., 2014), which has been chosen because it contains several heavy precipitation events over Italy (Ferretti et al., 2014).

In the RAMS-3DVar, the background error matrix is divided in three components along the three spatial directions (*x, y, z*). The $\mathbf{B_x}$ and $\mathbf{B_y}$ matrices take into account for the spatial correlation of the background error. They are assumed Gaussian with length-scales between 20 and 30 km, depending on the vertical level. Again, these distances are computed using the NMC methods (Barker et al., 2012).

The $\mathbf{B_z}$ matrix contains the error for the water vapor mixing ratio, which is the control variable used in RAMS-3DVar. This error is about 2 g/kg at the surface and decreases with height. In particular, it is larger than 0.5 g/kg below 4 km, and less than 0.2 g/kg above 5 km.

It is noted that cross correlations among variables are neglected in this study and the applications of the RAMS-3DVar affects the water vapor mixing ratio only.

Because the lightning data assimilation perturbs the water vapor mixing ratio, it follows that the data assimilation presented in this study changes only this parameter.

## 4. Results

### *4.1 Serano*

In this section we analyse two VSF forecasts of the Serano case. The first period (03-06 UTC) is the most intense, while the second period (18-21 UTC) corresponds to a rejuvenating phase of the storm.

#### *4.1.1 Serano: 03-06 UTC 16 November 2017*

In this period, an intense and localised storm hit the central Italy, while light precipitation occurred over northern Italy (Figure 14a). Considering the storm over central Italy, 10 raingauges observed more than 30 mm/3h, 6 more than 40 mm/3h, 3 more than 50 mm/3h and 1 more than 60 mm/3h, the maximum observed value being 63 mm/3h.

The CTRL forecast, Figure 14b, misses the storm over central Italy and underestimates considerably the precipitation over Northern Italy, giving unsatisfactory results.

The assimilation of the radar reflectivity factor improves the forecast, as shown by Figure 14c. In particular, RAD forecast shows localized precipitation (30-35 mm/3h) close to the area were the most abundant precipitation was observed. However, the maximum precipitation is underestimated. Another interesting improvement of the RAD forecast compared to CTRL is the precipitation over northern Italy, whose area is much more in agreement with observations compared to CTRL.

The precipitation forecast given by LIGHT, Figure 14d, shows some improvements compared to CTRL because the precipitation over central Italy has a maximum of 25-30 mm/3h, close to the area where the maximum precipitation was observed. LIGHT, however, has a worse performance compared to RAD because it misses the light precipitation over northern Italy. Also, similarly to RAD, LIGHT underestimates the maximum precipitation.

RADLI forecast, Figure 14e, shows the best performance. The precipitation over central Italy is better represented because the maximum rainfall (40-45 mm/3h) is in reasonable agreement with observations, and also because the area with intense precipitation (> 25 mm/3h) is elongated in the SW-NE direction in agreement with raingauge measurements, giving a much better idea of the real storm intensity compared to RAD and LIGHT, as well as CTRL. The light precipitation over northern Italy is well represented by RADLI.

Figure 14f shows the POD, computed for the domain of Figure 14a, for the time period considered. CTRL and LIGHT show a poor forecast compared to RAD and RADLI, underlining the importance of the assimilation of reflectivity factor observations for this phase of the storm. The POD of RADLI is 0.33 for the 30 mm/3h threshold (3 stations out of 10 where correctly predicted). This represents a good performance considering that the intense precipitation is localized and we used the nearest neighbour methodology to compute the score, which, for the specific grid resolution, limits to 5.7 km the displacement error.

Figure 14f also shows the significant improvement of RAD and RADLI for the light rainfall forecast because the POD for the 0.2 mm/3h threshold increases from 0.5 of CTRL (0.55 for LIGHT) to about 0.85 for both RAD and RADLI.

The ETS score shows again the positive impact of the data assimilation, especially radar reflectivity factor, on the rainfall forecast for this phase of the storm, the best performance given by RADLI.

The proportion of correct forecast, Figure 14h, is larger than 84% for all configurations. HR, however, is lower for RAD and RADLI compared to other configurations because of the larger number of false alarms given by the assimilation of radar reflectivity factor.

It is finally remarked that lightning and reflectivity factor data assimilation acted synergistically because the simulation assimilating both data performs much better than the simulations assimilating only one kind of observation, either radar reflectivity factor or lightning.

*4.1.2 Serano: 18-21 UTC 16 September 2017*

In this phase, rainfall occurred mainly over central Italy with moderate-heavy amounts. In particular, 51 raingauges measured more than 10 mm/3h, 13 more than 20 mm/3h, 3 more than 30 mm/3h and 2 between 40 mm/3h and 50 mm/3h (Figure 15a). Rainfall was also observed over north-western Italy with 12 raingauges observing more than 10 mm/3h, 7 more than 20 mm/3h, 4 more than 30 mm/3h, and 3 between 40 mm/3h and 50 mm/3h.

The CTRL forecast, Figure 15b, shows little precipitation over central Italy, giving an unsatisfactory forecast, while the forecast over north-western Italy is well represented even if displaced few tens of kilometres to the North of the real occurrence.

The RAD forecast, Figure 15c, is better than CTRL. Firstly, the rainfall pattern over central Italy is well predicted but the maximum values are underestimated; secondly, the rainfall over north-western Italy is simulated more to the South compared to CTRL, more in agreement with observations.

The LIGHT forecast, Figure 15d, improves considerably the rainfall prediction over central Italy and the maximum values forecast by LIGHT are more in agreement with observations compared to RAD. The rainfall over north-western Italy is shifted to the North compared to raingauges measurements, similarly to CTRL.

RADLI forecast, Figure 15e, shares features with both RAD and LIGHT. For example, the maximum values over central Italy are similar to LIGHT, while the rainfall over north-western Italy is similar to RAD.

It is also noted that the precipitation over central Italy for thresholds higher than 20 mm/3h covers a wider area compared to LIGHT, extending towards the SW, giving a better representation of the observed precipitation.

RADLI has the best POD among the simulations, ranging from 0.8 (0.2 mm/3h) to 0.2 (38 mm/3h), followed by LIGHT and RAD. The improvement given by data assimilation to the CTRL forecast is notable for all experiments assimilating data (radar reflectivity factor and/or lightning). The ETS score shows that RADLI and LIGHT forecasts are useful up to about 40 mm/3h, while RAD forecast has a lower performance. Again, ETS shows a significant improvement of the simulations with data assimilation compared to CTRL. Despite the higher POD, RADLI has a lower ETS than LIGHT. This behaviour is found also for other VSF and is caused by the larger number of false alarms in the RADLI forecast, especially when compared to LIGHT.

The proportion of correct forecast (Figure 15h) is larger than 75% for all thresholds. The larger number of false alarms given by RADLI and RAD compared to LIGHT is notable in the lower values of HR for the configurations assimilating radar reflectivity factor.

Despite the bigger number of false alarms, the forecast given by RADLI is the best among all forecasts, because it clearly shows the moderate precipitation occurring over central and north-western Italy.

*4.2 Livorno*

The Livorno case lasted for several hours starting at 18 UTC on 9 September 2017 and ending more than a day later. The most intense phase in Livorno and its surroundings was observed during the night between 9 and 10 September. In the following, we will show three representative VSF (3h), including the most intense phase in Livorno.

*4.2.1 Livorno: 18-21 UTC 9 September 2017*

During this period, the precipitation started to hit intensely Livorno and its surroundings (point A in the Figure 16a). Figure 16a shows the rainfall observed between 18 and 21 UTC on 9 September. Over Tuscany there are three stations around Livorno (the yellow-red raingauges of Figure 16a close to label A) reporting more than 30 mm/3h: 31 mm/3h, 37 mm/3h, and 55 mm/3h, respectively. The precipitation is spread over Liguria, Tuscany and Emilia Romagna, with 130 raingauges, of the 517 raingauges available in this time interval, measuring more than 10 mm in 3h and 25 raingauges measuring more than 20 mm in 3h.

CTRL forecast for this period is shown in Figure 16b. It is apparent that CTRL misses the precipitation over coastal Tuscany, while that over the Apennines (label B in Figure 16a) is underestimated. CTRL predicts the precipitation over Liguria but the amount is overestimated being the forecast amount over 75 mm/3h for some stations, while observations have maximum values between 25 mm/3h and 30 mm/3h.

Figure 16c shows the RAD precipitation forecast. The impact of the reflectivity factor data assimilation is notable. Compared to CTRL, the precipitation covers a larger area and reaches the coastal part of Tuscany. The precipitation over Livorno is not well predicted, the amount being 10-15 mm/3h.

The precipitation over Liguria is still overestimated by RAD but to a lower extent compared to CTRL. The assimilation of radar reflectivity factor can increase or decrease the water vapour content of the simulations, depending on the reflectivity factor observed and simulated, and the lower precipitation over Liguria for RAD compared to CTRL is an effect of the reduction of water vapor caused by the data assimilation of radar reflectivity factor.

Figure 16d shows the precipitation simulated by LIGHT. The rainfall reaches the Tuscany coast and extends more to the East in the northern part of the domain compared to both CTRL and RAD, being LIGHT more in agreement with observations.

The precipitation forecast around Livorno is 25-30 mm/3h, however the precipitation over the sea, 30 km far from the location of the most intense precipitation observed in the 3h, reaches 45 mm in 3h, giving the hint of a potentially intense storm.

The rainfall over Liguria is overestimated by LIGHT, but to a less extent compared to both RAD and CTRL. The LIGHT simulation moves the storm southeastward faster than other configurations, leaving less rain over Liguria compared to RAD and CTRL.

Figure 16e shows the rainfall of RADLI forecast. The precipitation field shares some characteristics with the LIGHT simulation and some others with RAD simulation. For example, the precipitation in the northern part of the domain, similarly to LIGHT, extends more to the East compared to RAD. The precipitation swath over Tuscany coast is similar to that of RAD, but shifted southward. The maximum precipitation in the Livorno area is 20-25 mm /3h, underestimating the observed maximum precipitation, but being closer to the observed position compared to RAD. The precipitation over Liguria is overestimated by RADLI.

POD score, Figure 16f, shows that CTRL performance is improved by data assimilation. LIGHT performs better than RAD up to 16 mm/3h, while RAD performs better for larger thresholds, thanks to a better simulation of the precipitation over the Apennines (label B of Figure 16a). Interestingly, the POD of RADLI follows LIGHT up to 16 mm/3h and RAD for larger thresholds, having, overall, the best score.

ETS score, Figure 16g, confirms the results of POD. CTRL forecast is useful (ETS > 0) up to 14mm/3h, LIGHT up to 18 mm/3h, RAD and RADLI up to 22 mm/3h.

HR is lower for CTRL up to 22 mm/3h because it has a lower number of hits. For larger thresholds RADLI has the lowest HR because of its higher number of false alarms compared to other configurations.

In summary, for the period of the onset of high precipitation over Livorno, the assimilation of lighting or radar reflectivity factor or both data improves the precipitation forecast giving hint of intense precipitation in the Livorno area for both LIGHT and RADLI simulations. However, the maximum precipitation in Livorno is underestimated by the VSF forecast even with data assimilation, while the precipitation over Liguria is overestimated.

*4.2.2 Livorno: 00-03 UTC 10 September 2017*

This period represents the most intense phase of the storm in Livorno. In particular, the raingauge close to the label A (Figure 17a) reported 151 mm/3h (Collesalvetti), while the one close to the label B measured 82 mm/3h. Among the 518 raingauges reporting valid data, 75 observed more than 10 mm/3h, 31 more than 20 mm/3h, 17 more than 30 mm/3h, 9 more than 40 mm/3h, and 6 more than 50 (also 60) mm/3h.

The CTRL precipitation forecast is shown in Figure 17b. The forecast is poor because it misses the precipitation swath from the coast towards NE. Indeed, a precipitation swath is forecast about 50 km to the North of the real occurrence, but it is less wide compared to the observations.

The forecast of RAD, Figure 17c, shows that the assimilation of radar reflectivity factor gives a clear improvement to the forecast. The largest precipitation in the coastal part of the swath (we searched the maximum value in the area with longitudes between 10.20E and 10.70E and latitudes between 43.10N and 43.60N) is 94 mm/3h, clearly showing the occurrence of a heavy precipitation event. Another local maximum is shown in the southern part of the domain (label B). The maximum location is well represented, but the forecast value is 55 mm/3h while the observed maximum is 82 mm/3h.

An improvement, compared to both CTRL and RAD, is given by the assimilation of lightning (Figure 17d). Also for this simulation there is a precipitation swath from coastal Tuscany to the Apennines, but the shape of the swath better resembles that observed compared to RAD. The maximum value close to Livorno, i.e. in the coastal part of the swath, is 158 mm/3h, clearly showing the occurrence of a severe storm.

The LIGHT simulation also shows the local maximum in the southern part of the domain (about 50 mm/3h), but the amount is underestimated.

Figure 17e shows the rainfall forecast by RADLI. The precipitation swath from coastal Tuscany towards NE is more apparent compared to LIGHT and RAD. The maximum rain accumulated close to Livorno is 186 mm/3h. Also, the second precipitation maximum in the southern part of the domain reaches 70 mm/3h in good agreement with observations (82 mm/3h). Also, RADLI is the only run producing a satisfactory precipitation field over the south-eastern Emilia Romagna (north-eastern part of the domain), on the lee of the Apennines.

It is also noted that the main precipitation swath forecast by RADLI is too broad in the direction crossing the swath compared to the observations. This is confirmed by the FBIAS of RADLI (not shown), which is more than 3 for thresholds larger than 42 mm/3h.

Considering the POD, Figure 17f, we note the considerable improvement given to the score by data assimilation (lightning and/or radar reflectivity factor). POD is larger than 0.5 for RADLI and LIGHT up to the 52 mm/3h thresholds, clearly showing that those two configurations are able to catch the position and timing of the very intense precipitation, especially considering that the maximum displacement error for the precipitation field is 1.9 km.

RAD has a lower capability to correctly forecast the precipitation inland compared to FLASH and RADLI, however: a) it qualitatively reveals the heavy precipitation occurring in the Livorno area; b) the POD score is considerably improved compared to CTRL.

The ETS score, Figure 17g, underlines the good performance of RAD, LIGHT and RADLI compared to CTRL. RAD has a useful forecast (ETS > 0) up to 42 mm/3h, while LIGHT and RADLI show useful forecast up to 60 mm/3h. The lower ETS of RADLI compared to LIGHT for thresholds larger than 42 mm/3h is caused by the greater number of false alarms occurring in RADLI. The large variations of the scores for thresholds above 40 mm/3h is caused by the low number of raingauges observing those rainfall amounts.

CTRL ha the lowest HR, Figure 17h, up to 16 mm/3h because of the lower number of hits compared to other configurations. For thresholds larger than 32 mm/3h RADLI has the lowest HR due to the comparatively higher number of false alarms.

In summary, for the most intense precipitation period over Livorno, the data assimilation of lightning and radar reflectivity factor plays a key role for the correct representation of the storm intensity, timing and position, giving an improvement of paramount practical importance.

*4.2.3 Livorno: 06-09 UTC 10 September 2017*

In this period, the most intense phase of the precipitation occurred over Central Italy, over the coastal part of Lazio (Figure 18a). More in detail, among the 2695 raingauges reporting valid data over the domain of Figure 18a, 307 reported more than 10 mm/3h, 132 more than 20 mm/3h, 86 more than 30 mm/3h, 66 more than 40 mm/3h, 49 more than 50 mm/3h and 35 more than 60 mm/3h. Among the 35 raingauges measuring more than 60 mm/3h, 33 were over the Lazio, showing the heavy rainfall occurred over the Region.

Some precipitation persisted over Tuscany but the rainfall is much lower compared to previous 6h (the rainfall over Tuscany between 03 and 06 UTC was very intense, not shown). Other notable precipitation areas are over the NE of Italy (moderate to low amounts), over Central Alps (moderate values) and over the whole Sardinia (small amounts).

Figure 18b shows the rainfall simulated by CTRL. The forecast is unsatisfactory, mainly for the following two reasons: a) heavy precipitation is simulated over Tuscany (> 75 mm/3h), also close to the Livorno area; b) very small precipitation is forecast over Central Italy. The rainfall over NE

Italy is well represented in space, but overestimated because the forecast is higher than 50 mm/3h in correspondence of some raingauges, while observed values are 20-25 mm/3h. The small precipitation over Sardinia is not forecast by CTRL.

Considering the evolution of CTRL rainfall forecast for the different phases of the storm, we conclude that CTRL was able to predict abundant rain over Livorno, but this was delayed compared to the real event.

The rainfall simulated by RAD (Figure 18c) clearly improves the forecast compared to CTRL. First, the precipitation over Lazio is very well predicted and the rainfall values are higher than 40 mm/3h (up to 65 mm/3h), so the RAD forecast well represents the main precipitation spot over Italy for this period of time. Second, the precipitation over Tuscany is lowered compared to CTRL, showing the ability of radar reflectivity factor data assimilation to dry the model when it predicts rain that is not observed. Third, the precipitation over Central Alps is represented, even if located about 30 km to the East.

There are also aspects of the rainfall forecast that are less satisfactory: the small precipitation over Sardinia is not represented by RAD; the precipitation over NE Italy is well represented in space but overestimated.

LIGHT forecast, Figure 18d, shows a worse performance compared to RAD for this time period. The precipitation forecast is mainly over Tuscany, where it is overestimated, with a small precipitation spot over Lazio. There are, however, three improvements compared to CTRL and RAD: a) the small precipitation over Sardinia is well represented in LIGHT; b) the precipitation over Central Alps is well predicted; c) the rainfall forecast over NE Italy is overestimated by LIGHT but to a less extent compared to RAD.

The precipitation forecast of RADLI, Figure 18e, represents very well the precipitation over Lazio, and the rainfall amount is better predicted compared to RAD. The precipitation over Sardinia is well represented by RADLI as well as the precipitation over Central Alps, giving the best results among all forecasts.

The POD score (Figure 18f) confirms the above analysis. All the experiments with data assimilation outperform the CTRL forecast, and, for this time period, RAD performs better than LIGHT. RADLI shows the best POD among all configurations because it represents better the amount of rainfall over Lazio.

Similar considerations apply to ETS (Figure 18g); it is worth of note the high value of ETS for thresholds larger than 50 mm/3h, which represent heavy rainfall. Again, a forecast that was missed by CTRL is correctly represented by the assimilation of both radar reflectivity factor and lightning.

The HR score (Figure 18h) shows that CTRL has the lowest score for thresholds below 14 mm/3h because it has a lower number of hits. For higher thresholds (> 32 mm/3h), the impact of the false alarms become important and RADLI has the lowest HR.

## 5. Discussion and Conclusions

In this paper we have shown the impact of the lightning and radar reflectivity factor data assimilation on the very short term forecast (3h) of precipitation for two cases occurred in Italy. We use the RAMS@ISAC model, whose 3DVar extension to the assimilation of radar reflectivity factor is shown in this paper.

The first case study occurred on 16 September 2017 and it is a moderate case with localised rainfall over Central Italy. It was chosen because the control forecast, i.e. without radar reflectivity factor or lightning data assimilation, missed the event. The second event, occurred on 9-10 September 2017, was characterised by exceptional rainfall over several parts of Italy. This event was partially represented by the control forecast. In particular, the forecast of the event was incorrect because: a) the control forecast was delayed compared to the observations; b) the control forecast missed the rainfall over central Italy (Lazio Region).

It is important to recall that the impact of the lightning data assimilation on the precipitation forecast of RAMS@ISAC was already studied for the HyMeX-SOP1 period (Federico et al., 2017a, 2017b), and a robust statistic is already available. The results of this study confirm the important role of the lightning data assimilation on the rainfall forecast for two case studies. However, considering the assimilation of radar reflectivity factor, and its combination with lightning data assimilation in RAMS@ISAC, the results of this paper are new.

Because we analysed only two case studies, no definitive conclusions can be derived on the performance of RAMS@ISAC for radar reflectivity factor data assimilation. There are, however, few points worth of mention.

The VSF performance of RAMS@ISAC is systematically improved by the assimilation of radar reflectivity factor. This improvement is of paramount importance for some specific VSF (for example for the 00-03 UTC for Livorno), when the control forecast missed the event while it was correctly predicted by radar reflectivity factor data assimilation. Sometimes the improvement of reflectivity factor data assimilation has a lower impact on the precipitation forecast, as for the period 18-21 UTC on 9 September 2017 (Livorno) or for the second stage (18-21 UTC) of the Serano case; however, also for these cases the assimilation of reflectivity improves the precipitation forecast.

Lightning and radar observations are different and both add value to the VSF. In particular, flashes are recorded when deep convection develops, while radar reflectivity factor is observed also for light stratiform rain. Flashes are available for the open sea, while radar reflectivity factor is confined to the range of the coastal radars in the network. Lightning have a seasonal dependence over Italy, with the maximum in summer and fall, while radar reflectivity factor is available in all seasons.

For the above reasons, the impact of the two kinds of data on the rainfall VSF is expected different. Some examples have been shown: the light precipitation over Northern Italy for Serano case is well forecast assimilating radar reflectivity factor, while it is not simulated assimilating flashes because they are too few in this area to force convection into the model; lightning data assimilation is able to better represent the deep convection occurring during the intense phase of the Livorno case (00-03 UTC), especially because it is able to force convection where it occurs, reducing false alarms. The last characteristic has been found in some others VSF of the case studies considered, and it is shown by the fact that the ETS score for LIGHT is sometimes the best among all simulations.

The model configuration assimilating both radar reflectivity factor and lightning (RADLI) is able to retain important features of both data assimilation. For example, the simulation of the Livorno case in the phase 06-09 UTC was able to simulate the heavy precipitation over Lazio thanks to the radar reflectivity factor data assimilation and the precipitation over Sardinia, as well as the moderate precipitation over Central Alps, thanks to the lightning data assimilation.

Another example of synergistic interaction between the two types of data assimilation was found for the most intense phase of the Serano case (03-06 UTC on 16 September 2017). In this period, the light precipitation over the Alps was forecast by RADLI because of the assimilation of radar reflectivity factor, while the localised precipitation maximum over Central Italy was better forecast thanks to the synergistic action of lightning and reflectivity factor data assimilation.

The property of RADLI to retain the precipitation forecast features of both data is shown by the POD score, which is the best, for most cases and thresholds, for RADLI.

Another interesting feature is the considerable improvement of the POD of RADLI compared to CTRL for the lowest threshold, showing the better ability of RADLI to predict the area where precipitation will occur at the short term.

It is also underlined that the data assimilated, both lightning and radar reflectivity factor, are produced operationally and available in real time and could be used for an operational implementation of the model.

All the above features are promising and deserve future studies to better understand the role of radar reflectivity factor and its interaction with lightning data assimilation to improve the precipitation forecast; there are, however, less satisfactory aspects of assimilating both radar reflectivity factor and lightning data. The RADLI forecast has more false alarms compared to RAD and LIGHT and this penalises the usefulness of RADLI forecast. This is shown by the lower ETS and HR score of RADLI, especially compared to LIGHT, for some thresholds and VSF, despite the larger values of the POD of RADLI.

The RADLI forecast can miss intense precipitation: this is shown, for example, by the VSF of 18-21 UTC on 9 September 2017 (Livorno), when RADLI underestimated the most intense phase of the storm in Livorno.

In addition to the acquisition of more case studies, there are two directions of future development of this work. The lightning data assimilation can be formulated by 3DVar, using a strategy similar to the radar reflectivity factor in which pseudo-profiles of relative humidity are first generated where flashes are recorded, and then those profiles are assimilated by 3DVar. This methodology was already reported in Fierro et al. (2016). The assimilation of both radar reflectivity factor and lightning using 3DVar will be explored in future studies.

Another important point to study is how long the innovations introduced by data assimilation lasts in the model forecast. While in this study we explored the VSF at 3h, future studies must explore longer time ranges. A similar study was performed for lightning data assimilation (Federico et al., 2017b), using a model set-up very similar to that used in this paper. Results showed that the lightning data assimilation gave a small and positive contribution to the precipitation forecast up to 24 h. However, the impact of data assimilation decreased rapidly, and the improvement of the rainfall forecast was significant after 6h, small after 12h and negligible after 24 h. A study considering both radar reflectivity factor and lightning should be performed to understand the resilience of the innovations introduced by data assimilation.

**ACKNOWLEDGMENTS**

This work is a contribution to the HyMeX program. Part of the computational time used for this paper was granted by the ECMWF (European Centre for Medium Weather range Forecast) though the special project SPITFEDE. LINET data were provided by Nowcast GmbH (https://www.nowcast.de/) within a scientific agreement between H.D. Betz and the Satellite Meteorological Group of CNR-ISAC in Rome.

This work was partially funded by the agreement between CNR-ISAC and the Italian Department of Civil Protection.

**References**

Alexander, G. D., Weinman, J. A., Karyampoudi, V. M., Olson, W. S., and Lee, A. C. L.: The effect of assimilating rain rates derived from satellites and lightning on forecasts of the 1993 superstorm, Mon. Weather Rev., 127, 1433–1457, 1999.

Barker, D. M., Huang, X.-Y., Liu, Z., Aulignè, T., Zhang, X., Rugg ,S., Ajjaji, R., Bourgeois, A., Bray, J., Chen ,Y., Demirtas, M.,. Guo, Y.-R, Henderson, T., Huang, W, Lin, H.C., Michalakes, J., Rizvi, S., and Zhang, X.: The Weather Research and Forecasting (WRF) Model's Community Variational/Ensemble Data Assimilation System: WRFDA. Bull. Amer. Meteor. Soc., 93, 831–843, 2012.

Barker, D.M., Huang, W., Guo, Y.-R., and Xiao, Q.N.: A Three-Dimensional Variational Data Assimilation System For MM5: Implementation And Initial Results, Monthly Weather Review, 132, 897-914, 2004.

Betz, H.-D., Schmidt, K., Laroche, P., Blanchet, P., Oettinger, P., Defer, E., Dziewit, Z., and Konarski, J.: LINET-an international lightning detection network in Europe, Atmos. Res., 91, 564– 573, 2009.

Buzzi, A. and Tibaldi, S.: Cyclogenesis in the lee of the Alps: A case study. Q.J.R. Meteorol. Soc., 104: 271-287. https://doi.org/10.1002/qj.49710444004, 1978.

Caumont, O., Ducrocq, V., Wattrelot, E., Jaubert, G., and Pradier-Vabre, S.: 1D+3DVar assimilation of radar reflectivity data: a proof of concept, Tellus A: Dynamic Meteorology and Oceanography, 62:2, 173-187, https://www.tandfonline.com/doi/abs/10.1111/j.1600-0870.2009.00430.x, 2010.

Chang, D. E., Weinman, J. A., Morales, C. A., and Olson, W. S.: The effect of spaceborn microwave and ground-based continuous lightning measurements on forecasts of the 1998 Groundhog Day storm, Mon. Weather Rev., 129, 1809–1833, 2001.

Chen, C. and Cotton, W.R.: A One-Dimensional Simulation of the Stratocumulus-Capped Mixed Layer, Boundary Layer Meteorology, 25, 289-321, 1983.

Cotton, W.R., Pielke Sr., R.A., Walko, R.L., Liston, G.E., Tremback, C.J., Jiang, H., McAnelly, R.L., Harrington, J.Y.m Nicholls, M.E., Carrio, G.G., and McFadden, J.P.: RAMS 2001: Current status and future directions, Meteorology and Atmospheric Physics, 82, 5-29,2003.

Courtier, P., Thépaut, J. N., and Hollingsworth, A.: A strategy for operational implementation of 4D-Var, using an incremental approach, Q. J. Roy. Meteorol. Soc., 120, 1367–1387, 1994.

Dahl, J. M. L., Höller, H., and Schumann, U.: Modeling the Flash Rate of Thunderstorms. Part II: Implementation. Monthly Weather Review, 139, 3112-3124, 2011.

Ducrocq, V., Braud, I., Davolio, S., Ferretti, R., Flamant, C., Jansa, A., Kalthoff, N., Richard, E., Taupier-Letage, I., Ayral, P.-A., Belamari, S., Berne, A., Borga, M., Boudevillain, B., Bock, O., Boichard, J.-L., Bouin, M.-N., Bousquet, O., Bouvier, C., Chiggiato, J., Cimini, D., Corsmeier, U., Coppola, L., Cocquerez, P., Defer, E., Delanoë, J., Di Girolamo, P., Doerenbecher, A., Drobinski, P., Dufournet, Y., Fourrié, N., Gourley, J.J., Labatut, L., Lambert, D., Le Coz, J., Marzano, F.S., Molinié, G., Montani, A., Nord, G., Nuret, M., Ramage, K., Rison, W., Roussot, O., Said, F., Schwarzenboeck, A., Testor, P., Van Baelen, J., Vincendon, B., Aran, M., and Tamayo, J.: HYMEX-SOP1 The Field Campaign Dedicated to Heavy Precipitation and Flash Flooding in the Northwestern Mediterranean. Bull. Amer. Meteor. Soc., 95, 1083–1100, https://doi.org/10.1175/BAMS-D-12-00244.1 , 2014.

Jones, C. D., and Macpherson, B.: A latent heat nudging scheme for the assimilation of precipitation into an operational mesoscale model, Meteorol. Appl., 4, 269–277, 1997.

Fabry, F., and Sun, J: For how long should what data be assimilated for the mesoscale forecasting of convection and why? Part I: On the propagation of initial condition errors and their implications for data assimilation. Monthly Weather Review, 138(1), 242–255, https://doi.org /2009mwr2883.1, 2010.

Federico, S., Petracca, M., Panegrossi, G., and Dietrich, S.: Improvement of RAMS precipitation forecast at the short-range through lightning data assimilation, Nat. Hazards Earth Syst. Sci., 17, 61–76, https://doi.org/10.5194/nhess-17-61-2017, 2017a.

Federico, S., Petracca, M., Panegrossi, G., Transerici, C., and Dietrich, S.: Impact of the assimilation of lightning data on the precipitation forecast at different forecast ranges. Adv. Sci. Res., 14, 187–194, 2017b.

Federico, S.: Implementation of the WSM5 and WSM6 Single Moment Microphysics Scheme into the RAMS Model: Verification for the HyMeX-SOP1, Advances in Meteorology, Volume 2016 , 2016.

Federico, S., Avolio, E., Petracca, M., Panegrossi, G., Sanò, P., Casella, D., and Dietrich S.:Simulating lightning into the RAMS model: Implementation and preliminary results, Natural Hazards and Earth System Sciences, Volume 14, Number 11, p.2933-2950, 2014.

Federico, S.: Implementation of a 3D-Var system for atmospheric profiling data assimilation into the RAMS model: Initial results, Atmospheric Measurement Techniques, 6(12), 3563-3576, 2013.

Ferretti, R., Pichelli, E., Gentile, S., Maiello, I., Cimini, D., Davolio, S., Miglietta, M. M., Panegrossi, G., Baldini, L., Pasi, F., Marzano, F. S., Zinzi, A., Mariani, S., Casaioli, M., Bartolini, G., Loglisci, N., Montani, A., Marsigli, C., Manzato, A., Pucillo, A., Ferrario, M. E., Colaiuda, V., and Rotunno, R.: Overview of the first HyMeX Special Observation Period over Italy: observations and model results, Hydrol. Earth Syst. Sci., 18, 1953–1977, https://doi.org/10.5194/hess-18-1953-2014, 2014.

Fierro, A. O., Mansell, E., Ziegler, C., and MacGorman, D.: Application of a lightning data assimilation technique in the WRFARW model at cloud-resolving scales for the tornado outbreak of 24 May 2011, Mon. Weather Rev., 140, 2609–2627, 2012.

Fierro, A.O., Gao, l., Ziegler, C. L., Calhoun, K. M., Mansell, E. R., and MacGorman, D. R.: Assimilation of Flash Extent Data in the Variational Framework at Convection-Allowing Scales: Proof-of-Concept and Evaluation for the Short-Term Forecast of the 24 May 2011 Tornado Outbreak. Mon. Wea. Rev., 144, 4373–4393,https://doi.org/10.1175/MWR-D-16-0053.1, 2016.

Giannaros, T. M., Kotroni, V., and Lagouvardos, K.: WRFLTNGDA: A lightning data assimilation technique implemented in the WRF model for improving precipitation forecasts, Environ. Model. Softw., 76, 54–68, doi:10.1016/j.envsoft.2015.11.017, 2016.

Hong, S.Y., Lim, J.J.O.: The WRF single-moment 6-class microphysics scheme (WSM6). J. Korean Meteorol. Soc. 42, 129–151, 2006.

Ikuta, Y. and Honda, Y.: Development of 1D+4DVAR data assimilation of radar reflectivity in JNoVA. Tech. Report, 01.09–01.10. http://www.wcrp-climate.org/WGNE/BlueBook/2011/individual-articles/01_Ikuta_Yasutaka_WGNE2011_1D4DVAR.pdf, 2011.

Jones, C. D., and Macpherson, B.: A latent heat nudging scheme for the assimilation of precipitation into an operational mesoscale model, Meteorol. Appl., 4, 269–277, 1997.

Kain, J. S. and Fritsch, J. M.: Convective parameterization for mesoscale models: the Kain-Fritsch scheme. The representation of cumulus convection in numerical models, Meteor. Monogr. No. 46, Am. Meteor. Soc., Boston, 165–170, 1993.

Kummerow, C., Hong, Y., Olson, W.S., Yang. S., Adler, R.F., McCollum, J., Ferraro, R., Petty, G., Shin. D.-B., and Wilheit, T.T.: The evolution of the Goddard profiling algorithm (GPROF) for rainfall estimation from passive microwave sensors. J. Appl. Meteor., 40, 1801–1820, 2001.

Maiello, I., Ferretti, R., Gentile, S., Montopoli, M., Picciotti, E., Marzano, F. S., and Faccani, C.: Impact of radar data assimilation for the simulation of a heavy rainfall case in central Italy using WRF–3DVAR, Atmos. Meas. Tech., 7, 2919-2935, https://doi.org/10.5194/amt-7-2919-2014, 2014.

Mansell, E. R., Ziegler, C. L., and MacGorman, D. R.: A lightning data assimilation technique for mesoscale forecast models, Mon. Weather Rev., 135, 1732–1748, 2007.

Mellor, G., and Yamada, T.: Development of a Turbulence Closure Model for Geophysical Fluid Problems, Review of Geophysics and Space Physics, 20, 851-875, 1982.

Molinari, J., and Corsetti, T.: Incorporation of cloud-scale and mesoscale down-drafts into a cumulus parametrization: results of one and three-dimensional integrations, Monthly Weather Review, 113, 485-501, 1985.

Olson, W. S., Kummerow, C. D. , Heymsfield, G. M., and Giglio, L.: A method for combined passive-active microwave retrievals of cloud and precipitation profiles. J. Appl. Meteor., 35, 1763-1789, 1996.

Parrish, D.F., and Derber, J.C.: The National Meteorological Center's Spectral Statistical Interpolation analysis system, Monthly Weather Review, 120, 1747-1763, 1992.

Qie, X., Zhu, R., Yuan, T., Wu, X., Li, W., and Liu, D.: Application of total-lightning data assimilation in a mesoscale convective system based on the WRF model, Atmos. Res., 145–146, 255–266, 2014.

Ridal, M., and Dahlbom, M.: Assimilation of multinational radar reflectivity data in a mesoscale model: a proof of concept, Journal of Applied Meteorology and Climatology, 56(6), 1739–1751. https://doi.org/10.1175/jamc-d-16-0247.1, 2017.

Skamarock, W. C., Klemp, J. B., Dudhia, J., Gill, D. O., Barker, D. M., Duda, M. G., Huang, X.-Y., Wang, W., and Powers, J. G.: A description of the Advanced Reasearch WRF Version 3. NCAR Technical Note, TN 475+STR, 113 pp., available at: http://www2.mmm.ucar.edu/wrf/users/docs/arw_v3.pdf (last access: November 2018), 2008.

Smagorinsky, J.: General circulation experiments with the primitive equations. Part I, The basic experiment, Monthly Weather Review, 91, 99-164, 1963.

Stensrud, D. J., and Fritsch, J. M.: Mesoscale convective systems in weakly forced large-scale environments. Part II: Generation of a mesoscale initial condition, Mon. Weather Rev., 122, 2068-2083, 1994.

Sun, J., and Crook, N. A.: Dynamical and Microphysical Retrieval from Doppler RADAR Observations Using a Cloud Model and Its Adjoint, Part I: Model Development and Simulated Data Experiments, J. Atmos. Sci., 54, 1642–1661, 1997.

Nat. Hazards Earth Syst. Sci. Discuss., https://doi.org/10.5194/nhess-2018-319
Manuscript under review for journal Nat. Hazards Earth Syst. Sci.
Discussion started: 23 November 2018

Natural Hazards and Earth System Sciences
Discussions

Sun, J., and Crook, N. A.: Dynamical and Microphysical Retrieval from Doppler RADAR Observations Using a Cloud Model and Its Adjoint, Part II: Retrieval Experiments of an Observed Florida Convective Storm, J. Atmos. Sci., 55, 835–852, 1998.

Sun, J. and Wang, H.: Radar data assimilation with WRF 4DVar. Part II: comparison with 3D-Var for a squall line over the US Great Plains, Mon. Weather Rev., 11, 2245–2264, https://doi.org/10.1175/MWR-D-12-00169.1, 2012.

Walko, R.L., Band, L.E., Baron, J., Kittel, T.G., Lammers, R., Lee, T.J., Ojima, D., Pielke Sr., R.A., Taylor, C., Tague, C., Tremback, C.J., and Vidale, P.L.: Coupled Atmosphere-Biosphere-Hydrology Models for environmental prediction, Journal of Applied Meteorology, 39, 931-944, 2000.

Wang, H., Sun, J., Zhang, X., Huang, X., and Auligne, T.: Radar data assimilation with WRF 4D-Var. Part I: system development and preliminary testing, Mon. Weather Rev., 141, 2224–2244, 2013.

Wattrelot, É., Caumont, O. and Mahfouf, J. F.: Operational implementation of the 1D+3D-Var assimilation method of radar reflectivity data in the AROME model. Monthly Weather Review, 142(5), 1852–1873. https://doi.org/10.1175/MWR-D-13-00230.1, 2014.

Weisman, M. L., Skamarock, W. C., and Klemp, J. B.: The resolution dependence of explicitly modeled convective systems, Mon.Weather Rev., 125, 527–548, 1997.

Weygandt, S. S., Benjamin, S. G., Hu, M., Smirnova, T. G., and Brown, J. M.: Use of lightning data to enhance radar assimilation within the RUC and Rapid Refresh models. Third Conf. on Meteorological Applications of Lightning Data, 20–24 January 2008, New Orleans, LA, Amer. Meteor. Soc., 8.4, available at: https://ams.confex.com/ams/88Annual/webprogram/Paper134112.html (last access: 03 October 2018), 2008.

Xiao, Q., Kuo, Y.-H., Sun, J., and Lee, W. C.: Assimilation of Doppler RADAR Observations with a Regional 3DVAR System: Impact of Doppler Velocities on Forecasts of a Heavy Rainfall Case, J. Appl. Meteor., 44, 768–788, 2005.

Xiao, Q., Kuo, Y.-H., Sun, J., Chaulee, W., and Barker, D. M.: An Approach of RADAR Reflectivity Data Assimilation and Its Assessment with the Inland QPF of Typhoon Rusa (2002) at Landfall, J. Appl. Meteor. Climatol., 46, 14–22, 2007.

Xu, Q., Wei, L., Gu, W., Gong, J., and Zhao, Q.: A 3.5-dimensional variational method for Doppler radar data assimilation and its application to phased array radar observations, Adv. Meteorol., vol. 2010, Article ID 797265, https://doi.org/10.1155/2010/797265, 2010.

Xue, M., Wang, D., Gao, J., Brewster, K., and Droegemeier, K. K: The Advanced Regional Prediction System (ARPS), storm scale numerical weather prediction and data assimilation, Meteor. Atmos. Phys., 82, 139–170, 2003.

Zhao, Q., Cook, J., Xu, Q., and Harasti, P. R.: Using radar wind observations to improve mesoscale numerical weather prediction, Weather Forecast, 21, 502–522, 2006.

## TABLES

Table 1: List of physical parameterisations used for RAMS@ISAC in this paper.

| Physical parameterization | Selected scheme |
|---|---|
| Parametrized cumulus convection | Modified Kuo scheme to account for updraft and downdraft (Molinari and Corsetti, 1985). The scheme is applied to R10 only. |
| Explicit precipitation parameterization | Bulk microphysics with six hydrometeors (cloud, rain, graupel, snow, ice, water vapor). Described in Hong and Lim (2006). |
| Exchange between the surface, the biosphere and atmosphere. | LEAF3 (Walko et al., 2000). LEAF includes prognostic equations for soil temperature and moisture for multiple layers, vegetation temperature and surface water, and temperature and water vapor mixing ratio of canopy air. |
| Sub-grid mixing | The turbulent mixing in the horizontal directions is parameterised following Smagorinsky (1963), vertical diffusion is parameterised according to the Mellor and Yamada (1982) scheme, which employs a prognostic turbulent kinetic energy. |
| Radiation scheme | Chen-Cotton (Chen and Cotton, 1983). The scheme accounts for condensate in the atmosphere. |

Table 2: Basic parameters of the RAMS@ISAC grids (R10, R4 and R1, corresponding, respectively, to the domains D1, D2 and D3). NNXP is the number of grid points in the WE direction, NNYP is the number of grid-points in the NS direction, NNZP is the number of vertical levels, DX is the size of the grid spacing in the WE direction, DY is the grid spacing in the SN direction. Lx, Ly, and Lz are the domain extensions in the NS, WE, and vertical directions. CENTLON and CENTLAT are the coordinates of the grid centres.

| | **R10, D1** | **R4, D2** | **R1, D3** |
|---|---|---|---|
| NNXP | 301 | 401 | 203 |
| NNYP | 301 | 401 | 203 |
| NNZP | 36 | 36 | 36 |
| Lx | 3000 km | 1600 km | ~270 km |
| Ly | 3000 km | 1600 km | ~270 km |
| Lz | ~22400 m | ~22400 m | ~22400 m |
| DX | 10 km | 4 km | 4/3 km |
| DY | 10 km | 4 km | 4/3 km |
| CENTLAT (°) | 43.0 N | 43.0 N | 43.7 N |
| CENTLON (°) | 12.5 E | 12.5 E | 11.0 E |

Nat. Hazards Earth Syst. Sci. Discuss., https://doi.org/10.5194/nhess-2018-319
Manuscript under review for journal Nat. Hazards Earth Syst. Sci.
Discussion started: 23 November 2018


Natural Hazards and Earth System Sciences
Open Access
Discussions

**FIGURES**

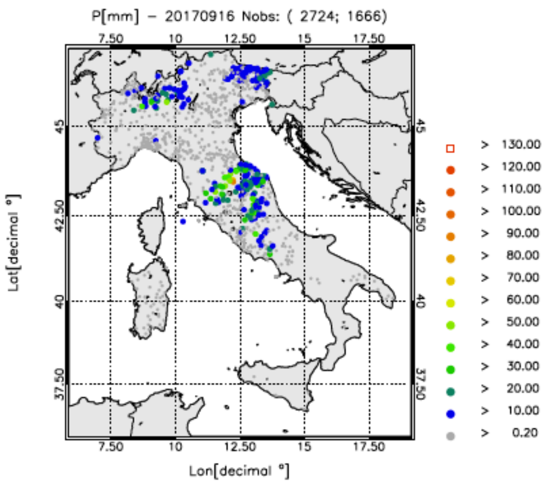


Figure 1: Daily precipitation (P) [mm] over Italy from the network of the Department of Civil Protection on 16 September 2017. Only raingauges observing at least 0.2 mm/day are shown. The first number in the figure title within brackets represents the available raingauges, while the second number represents raingauges observing at least 0.2 mm/3h. The lowest precipitation class is represented by smaller dots, the largest by a red square.

a)

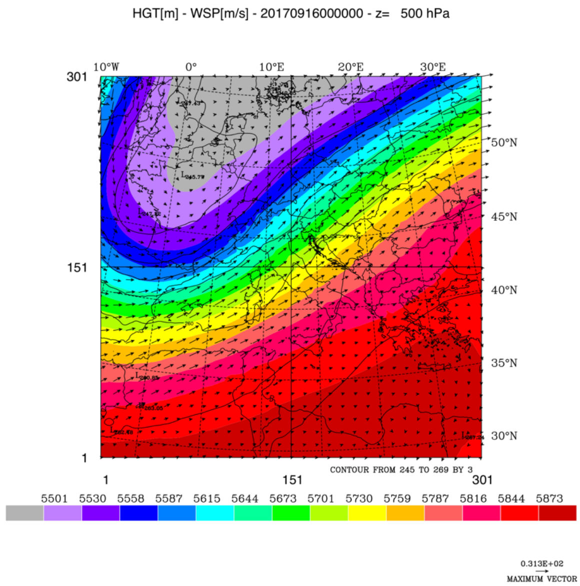


b)

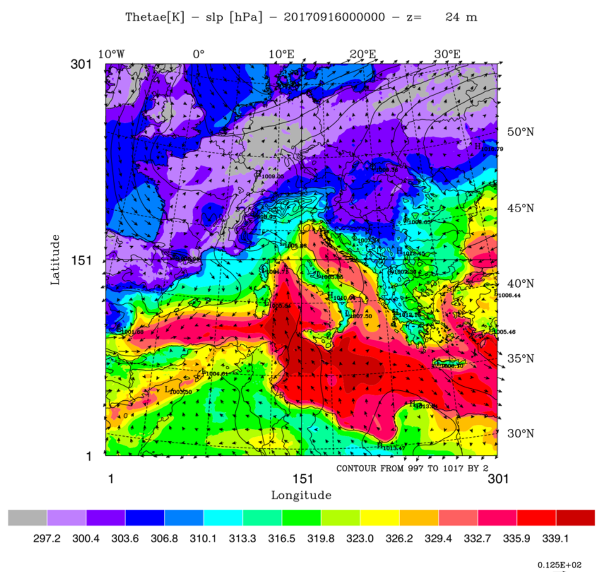


Figure 2: a) Geopotential height (filled contours), temperature (contours) and wind vectors at 500 hPa at 00 UTC on 16 September 2017. Maximum velocity is 31 m/s; b) equivalent potential temperature (filled contours), sea-level pressure (contours) and wind vectors at 24 m above the surface (first vertical level, maximum value 13 m/s). A low-pressure patter is forming over northern Italy, with a front in the western Mediterranean.

Nat. Hazards Earth Syst. Sci. Discuss., https://doi.org/10.5194/nhess-2018-319
Manuscript under review for journal Nat. Hazards Earth Syst. Sci.
Discussion started: 23 November 2018




a) b) c)

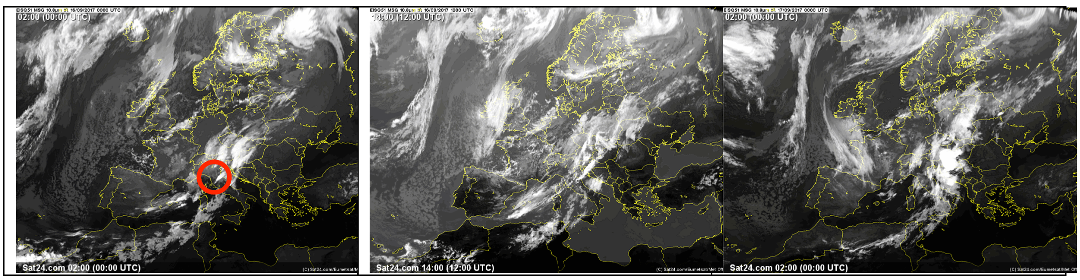


00UTC 16 sep 12UTC 16 sep 00UTC 17 sep

Figure 3: a) Satellite images (METEOSAT second generation) of the infrared channel, 10.8 micron, for 00 UTC and 12 UTC on 16 September, and for 00 UTC on 17 September 2017. A well-defined cloud system is apparent inside the red circle of the image at 00 UTC on 16 September 2017.

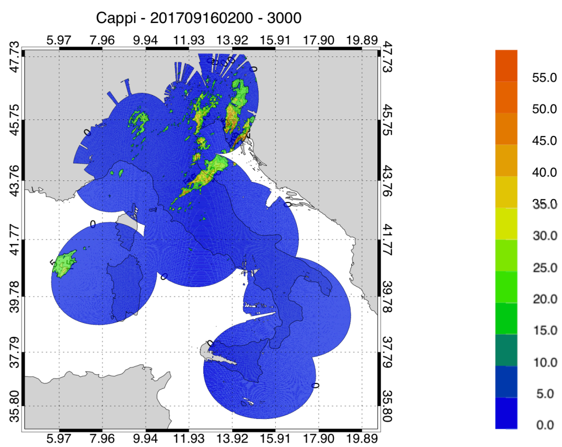


Figure 4: National radar mosaic at 3 km above the sea level observed at 02 UTC on 16 September 2017.

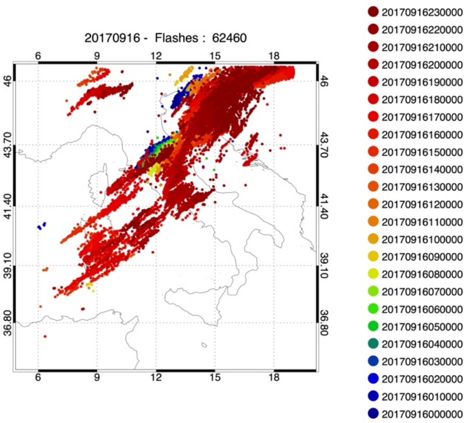


Figure 5: Lightning recorded on 16 September 2017. The total number of flashes recorded is shown in the title. Different colours represent the time (UTC) of occurrence of the lightning.

a) b)

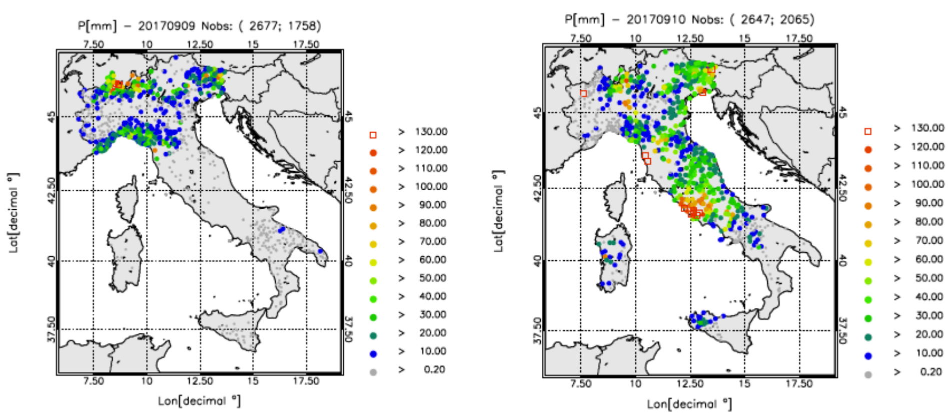


Figure 6: a) As in Figure 1 but for a) 9 September 2017 and b) 10 September 2017.

Nat. Hazards Earth Syst. Sci. Discuss., https://doi.org/10.5194/nhess-2018-319
Manuscript under review for journal Nat. Hazards Earth Syst. Sci.
Discussion started: 23 November 2018


Natural Hazards and Earth System Sciences
Discussions

a)

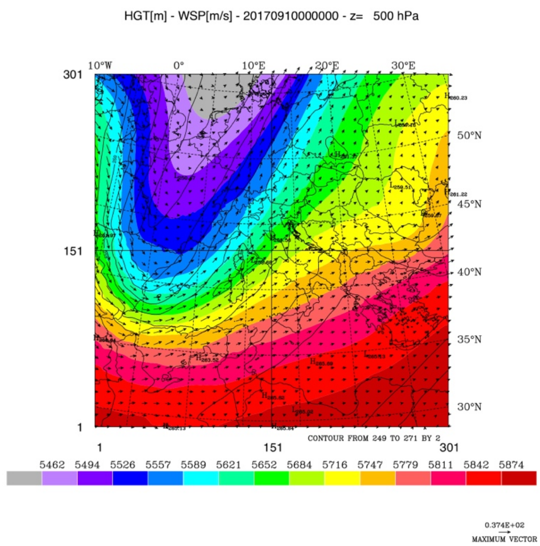


b)

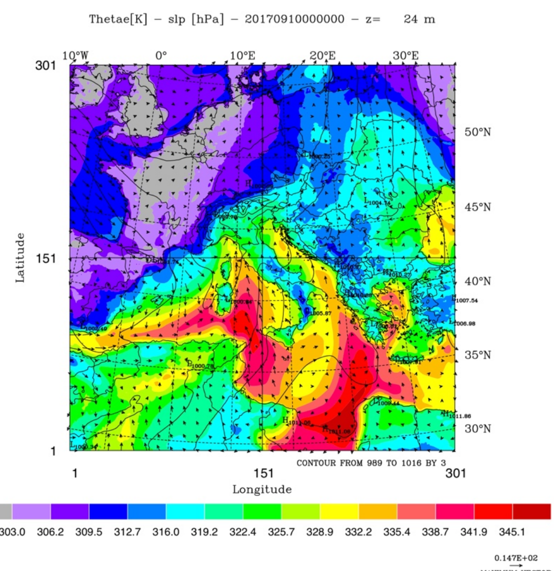


Figure 7: a) Geopotential height (filled contours), temperature (contours) and wind vectors at 500 hPa at 00 UTC on 10 September 2017. Maximum velocity is 37 m/s; b) equivalent potential temperature (filled contours), sea-level pressure (contours) and wind vectors at 24 m above the surface (first vertical level, maximum value 15 m/s).

Nat. Hazards Earth Syst. Sci. Discuss., https://doi.org/10.5194/nhess-2018-319
Manuscript under review for journal Nat. Hazards Earth Syst. Sci.
Discussion started: 23 November 2018


a) b)

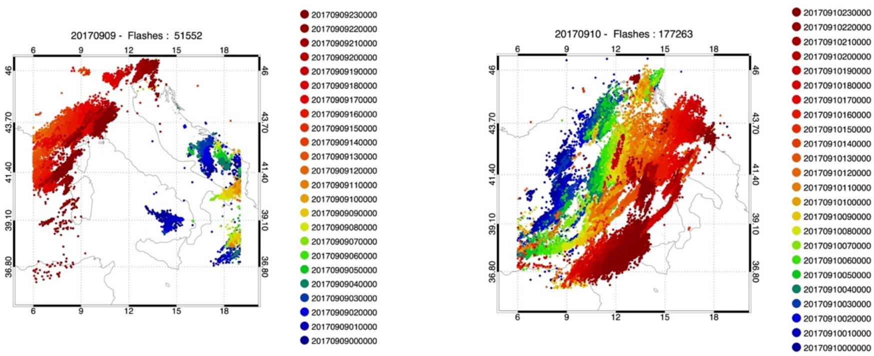


Figure 8: a) Lightning recorded on 09 September 2017; b) Lightning recorded on 10 September 2017. The number of flashes recorded on each day is shown in the title. Different colours represent the time of occurrence of the lightning.

a) b) c)

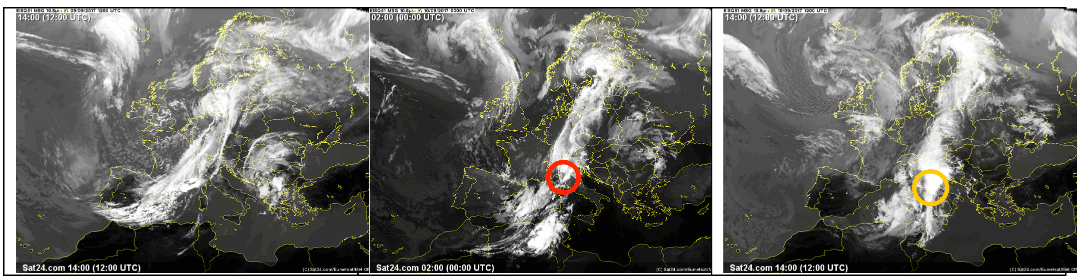


*12UTC 09 sep* *00UTC 10 sep* *12UTC 10 sep*

Figure 9: a) Satellite images (METEOSAT second generation) of the infrared channel, 10.8 micron, for 12 UTC on 9 September 2017, 00 UTC and 12 UTC on 10 September 2017.

Nat. Hazards Earth Syst. Sci. Discuss., https://doi.org/10.5194/nhess-2018-319
Manuscript under review for journal Nat. Hazards Earth Syst. Sci.
Discussion started: 23 November 2018

Natural Hazards and Earth System Sciences
Open Access
EGU
Discussions

a) b)

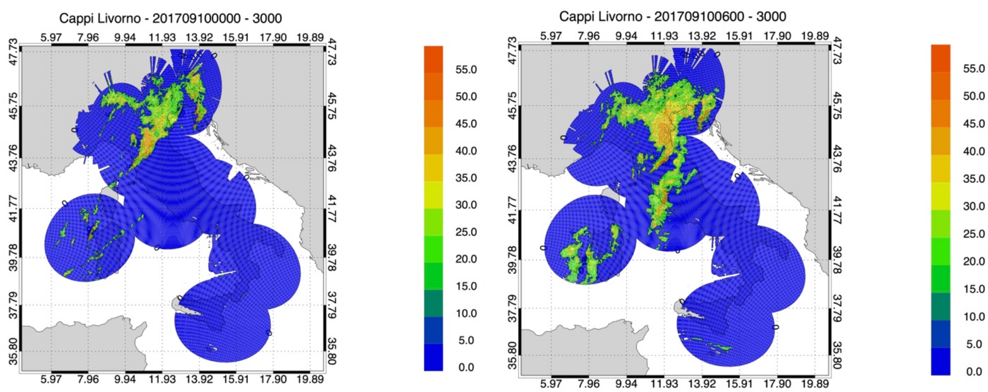


Figure 10: a) National radar mosaic at 3 km above the sea level observed at 00 UTC on 10 September 2017; b) as in a) for the 06 UTC.

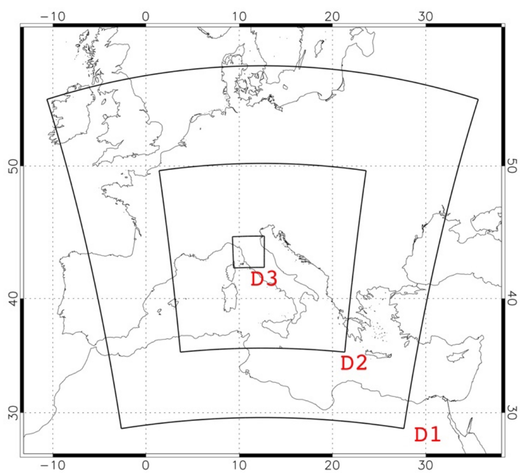


Figure 11: The three domains used in RAMS@ISAC.

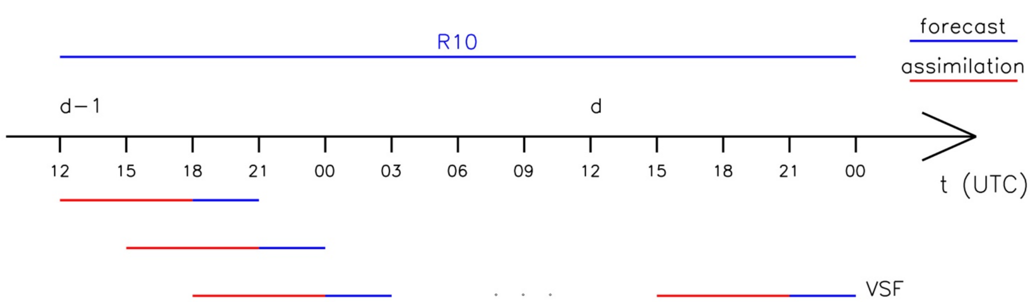


Figure 12: The time implementation of the RAMS@ISAC very short-term forecast.

Nat. Hazards Earth Syst. Sci. Discuss., https://doi.org/10.5194/nhess-2018-319
Manuscript under review for journal Nat. Hazards Earth Syst. Sci.
Discussion started: 23 November 2018


Natural Hazards and Earth System Sciences
Open Access
Discussions


Figure 13: The radar network of the Department of Civil Protection. Green radars operate with dual-polarisation, blue radars have single polarisation.

a)

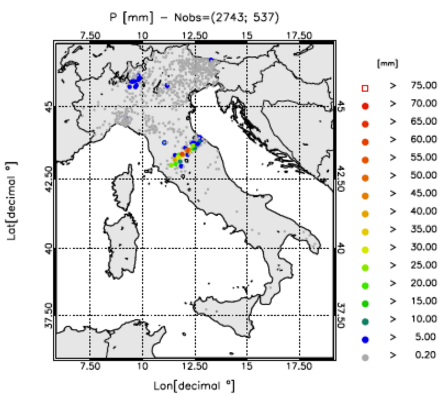


b)

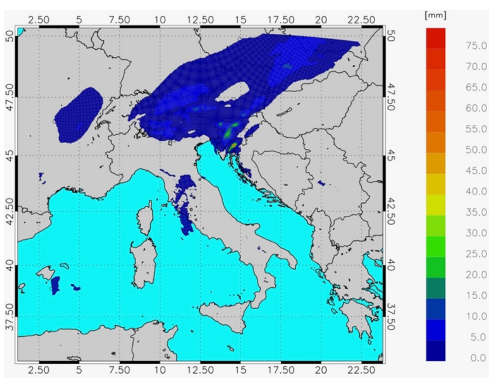


c)

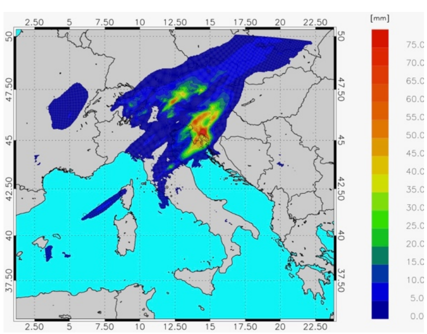


d)

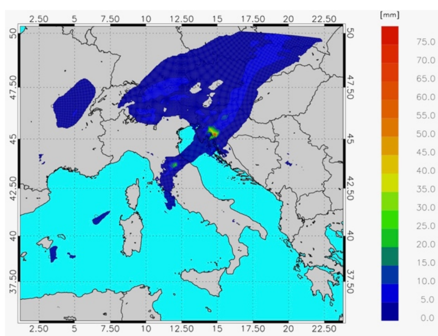

Nat. Hazards Earth Syst. Sci. Discuss., https://doi.org/10.5194/nhess-2018-319
Manuscript under review for journal Nat. Hazards Earth Syst. Sci.
Discussion started: 23 November 2018




e)

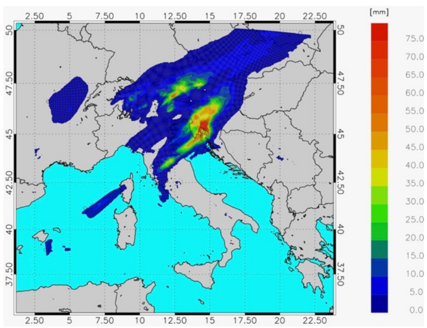


f)

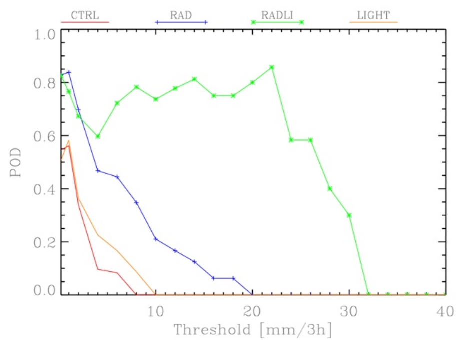


g)

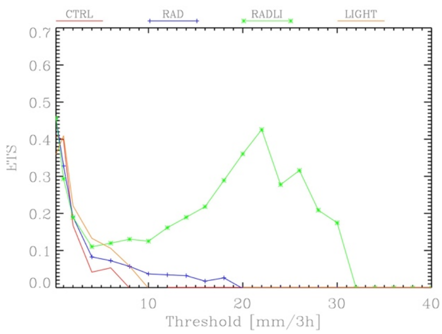


h)

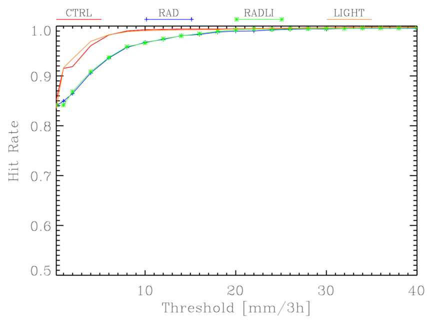


Figure 14: a) rainfall reported by raingauges between 03 and 06 UTC on 16 September 2017. Only raingauges observing at least 0.2 mm/day are shown. The first number in the title within brackets represents the available raingauges, while the second number represents those observing at least 0.2 mm/3h; b) as in a) for the CTRL forecast; c) as in a) for the RAD forecast; d) as in a) for the LIGHT forecast; e) as in a) for the RADLI forecast; f) POD score for the period 03-06 UTC on 16 September 2017; g) as in f) for the ETS score. POD and ETS scores are computed over the domain of Figure 14a.

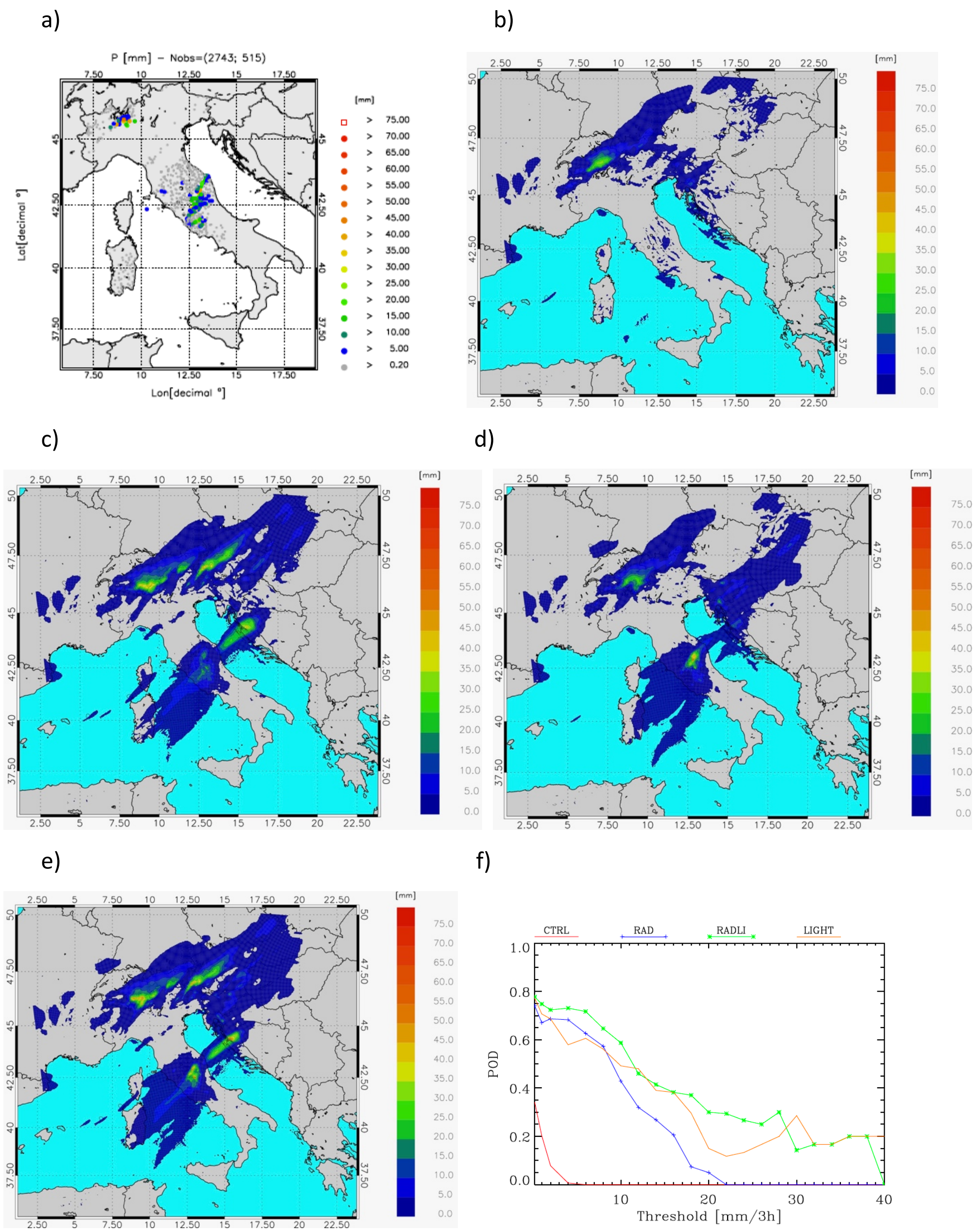
a)
b)
c)
d)
e)
f)
P [mm] – Nobs=(2743; 515)
Lat[decimal °]
Lon[decimal °]
[mm]
CTRL
RAD
RADLI
LIGHT
POD
Threshold [mm/3h]

Nat. Hazards Earth Syst. Sci. Discuss., https://doi.org/10.5194/nhess-2018-319
Manuscript under review for journal Nat. Hazards Earth Syst. Sci.
Discussion started: 23 November 2018


Natural Hazards and Earth System Sciences
Open Access
Discussions

g)

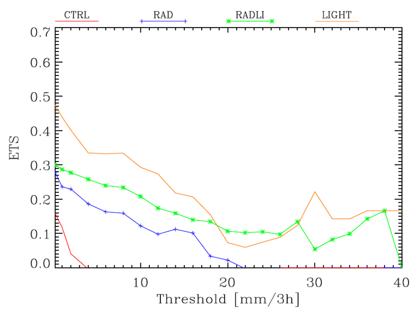


h)

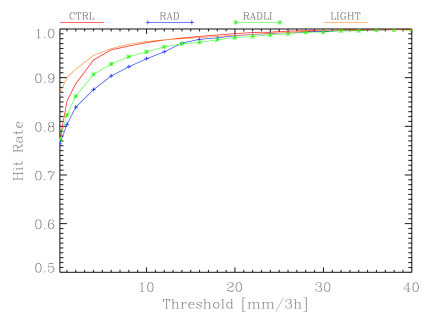


Figure 15: a) rainfall reported by raingauges between 18 and 21 UTC on 16 September 2017. Only raingauges measuring at least 0.2 mm/3h are shown. The first number in the title within brackets represents the available raingauges, while the second number represents those observing at least 0.2 mm/3h; b) as in a) for the CTRL forecast; c) as in a) for the RAD forecast; d) as in a) for the LIGHT forecast; e) as in a) for the RADLI forecast; f) POD score for the period 18-21 UTC on 16 September 2017; g) as in f) for the ETS score. POD and ETS scores are computed over the domain of Figure 15a.

a)

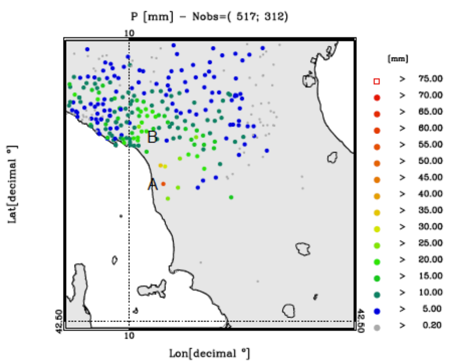


b)

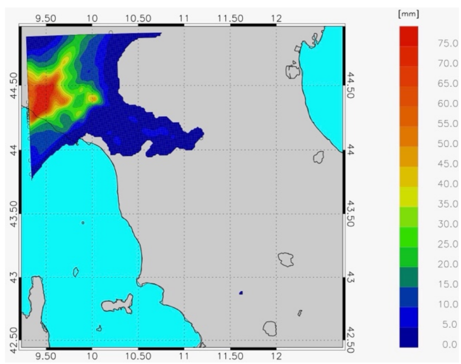


c)

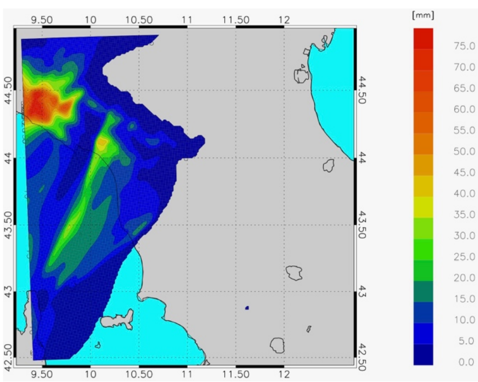


d)

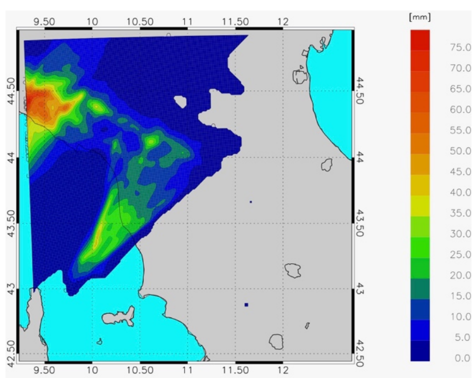

Nat. Hazards Earth Syst. Sci. Discuss., https://doi.org/10.5194/nhess-2018-319
Manuscript under review for journal Nat. Hazards Earth Syst. Sci.
Discussion started: 23 November 2018

Natural Hazards and Earth System Sciences
Open Access
Discussions

e)

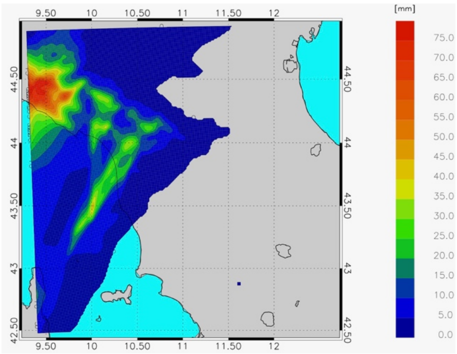


f)

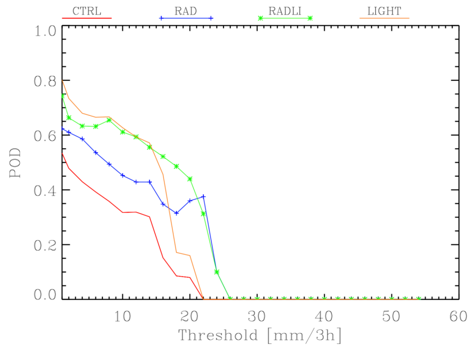


g)

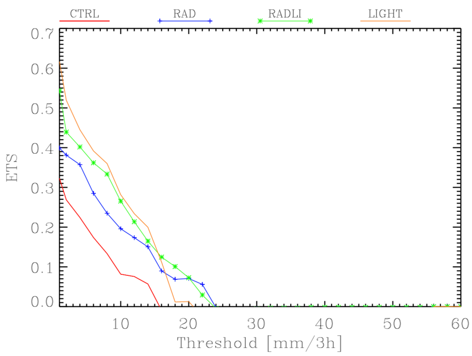


h)

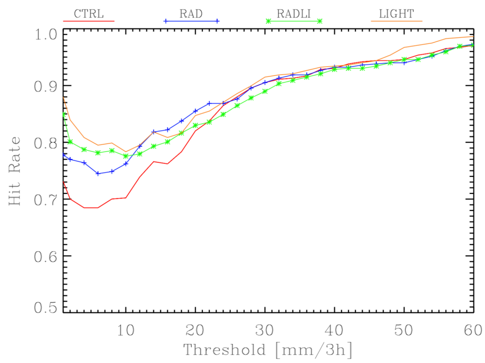


Figure 16: a) rainfall reported by raingauges between 18 and 21 UTC on 9 September 2017. Only raingauges observing at least 0.2 mm/3h are shown. The first number in the title within brackets represents the available raingauges, while the second number represents those observing at least 0.2 mm/3h; b) as in a) for the CTRL forecast; c) as in a) for the RAD forecast; d) as in a) for the LIGHT forecast; e) as in a) for the RADLI forecast; f) POD score for the period 18-21 UTC on 9 September 2017; g) as in f) for the ETS score. Label A in Figure 16a shown the position of Livorno. POD and ETS scores are computed over the domain of Figure 16a.

a)

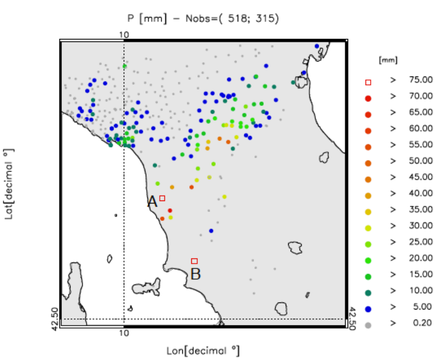


b)

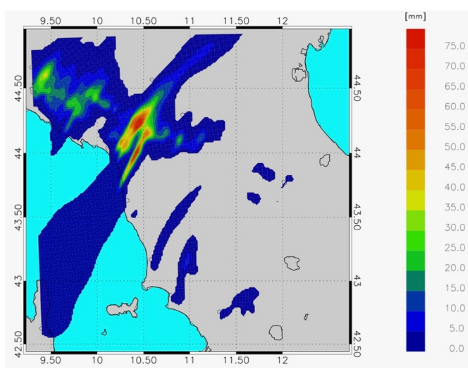

Nat. Hazards Earth Syst. Sci. Discuss., https://doi.org/10.5194/nhess-2018-319
Manuscript under review for journal Nat. Hazards Earth Syst. Sci.
Discussion started: 23 November 2018




c)

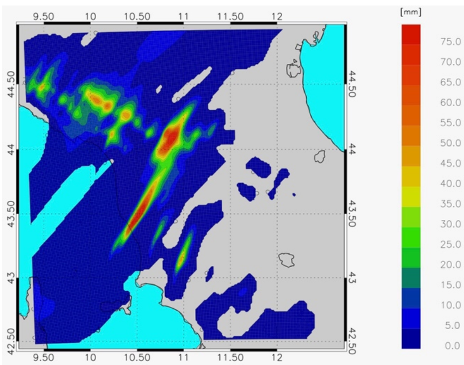


d)

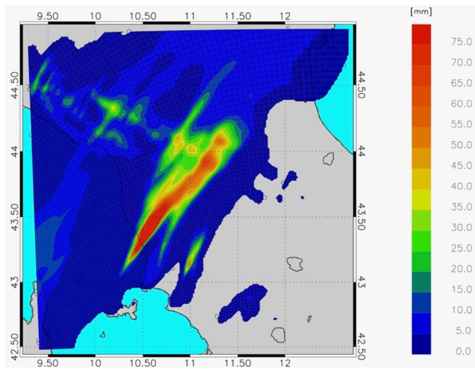


e)

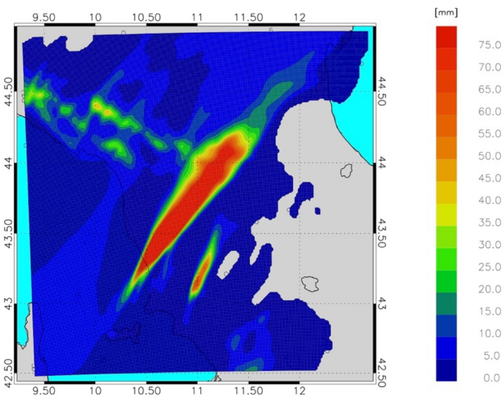


f)

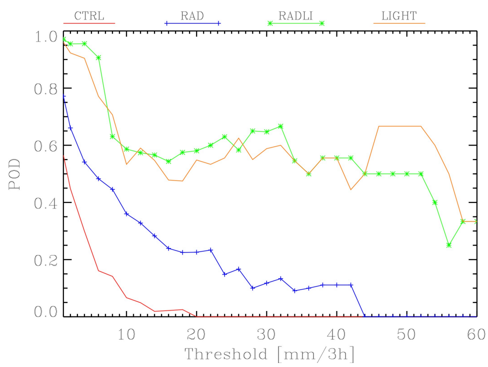


g)

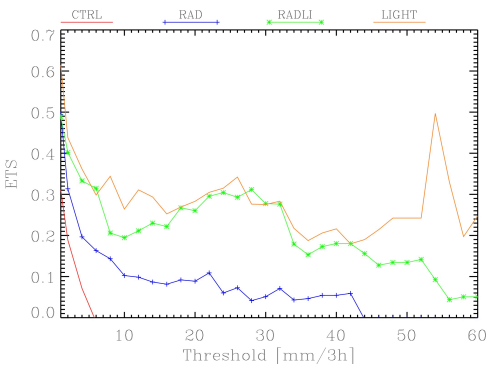


h)

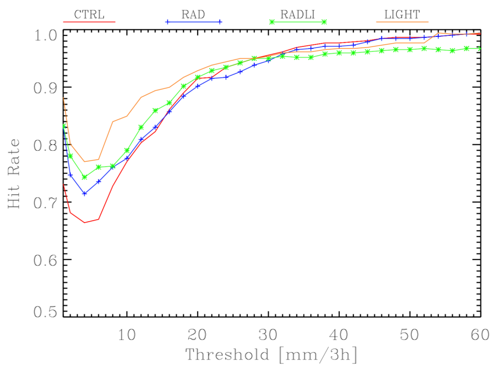

Nat. Hazards Earth Syst. Sci. Discuss., https://doi.org/10.5194/nhess-2018-319
Manuscript under review for journal Nat. Hazards Earth Syst. Sci.
Discussion started: 23 November 2018


Natural Hazards and Earth System Sciences
Open Access
Discussions

Figure 17: a) rainfall reported by raingauges between 00 and 03 UTC on 10 September 2017. Only stations reporting at least 0.2 mm/3h are shown. The first number in the title within brackets represents the number of raingauges available over the domain, while the second number shows those observing at least 0. 2 mm/3h; b) as in a) for the CTRL forecast; c) as in a) for the RAD forecast; d) as in a) for the LIGHT forecast; e) as in a) for the RADLI forecast; f) POD score for the period 00-03 UTC on 10 September; g) as in f) for the ETS score. POD and ETS scores are computed over the domain of Figure 17a.

a)

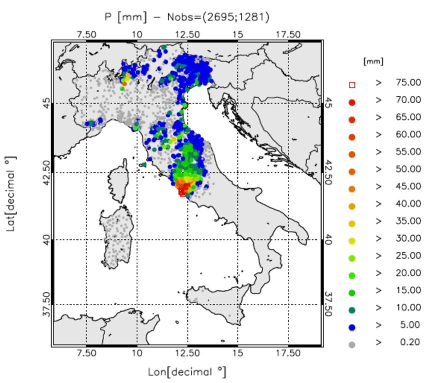


b)

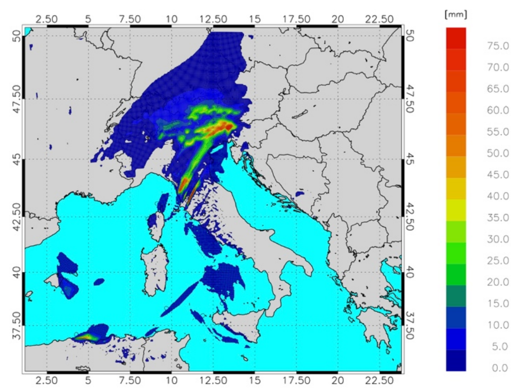


c)

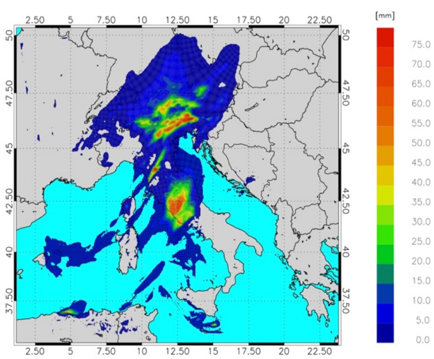


d)

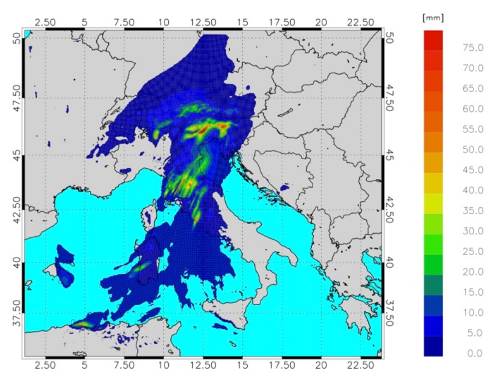

Nat. Hazards Earth Syst. Sci. Discuss., https://doi.org/10.5194/nhess-2018-319
Manuscript under review for journal Nat. Hazards Earth Syst. Sci.
Discussion started: 23 November 2018


Natural Hazards and Earth System Sciences
Discussions
Open Access

e)

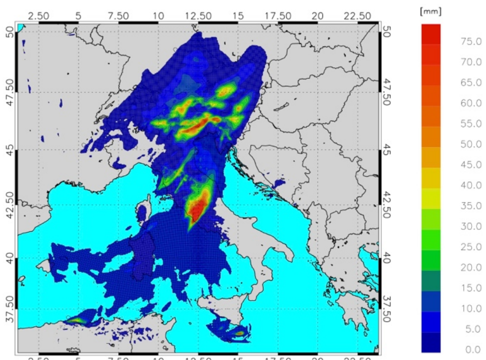


f)

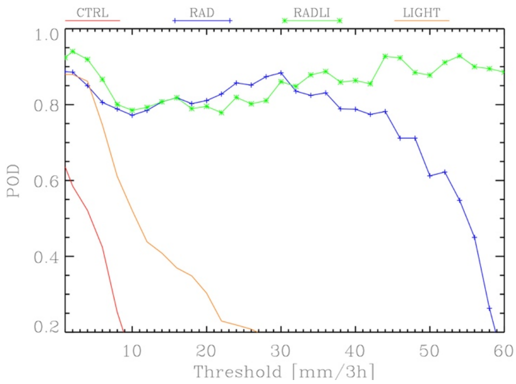


g)

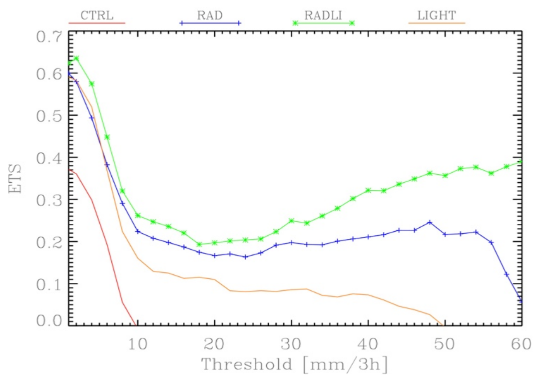


h)

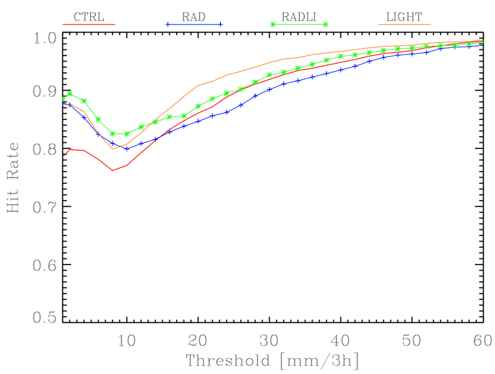


Figure 18: a) rainfall reported by raingauges between 06 - 09 UTC on 10 September 2017. For this time period 2695 raingauges reported valid observations in the domain, however only stations reporting at least 0.2 mm/3h are shown The first number in the title within brackets represents the number of raingauges available over the domain, while the second number shows those observing at least 0.2 mm/3h; b) as in a) for the CTRL forecast; c) as in a) for the RAD forecast; d) as in a) for the LIGHT forecast; g) as in a) for the RADLI forecast; f) POD score for the period 06-09 UTC on 10 September; e) as in f) for the ETS score. POD and ETS scores are computed over the domain of Figure 18a.